

CR 151526

SCATTEROMETER RECEIVER DYNAMIC
RANGE/LINEARITY
(SPE-S193-005, S&AD)

Job Order 75-215

(NASA-CR-151526) SCATTEROMETER RECEIVER
DYNAMIC RANGE/LINEARITY (Lockheed
Electronics Co.) 74 p HC A04/MF A01

N77-33481

CSCL 14B

Unclass

63/35

49702

Prepared by

Lockheed Electronics Company, Inc.
Aerospace Systems Division
Houston, Texas

Contract NAS 9-12200

for

EARTH OBSERVATIONS DIVISION



National Aeronautics and Space Administration
LYNDON B. JOHNSON SPACE CENTER

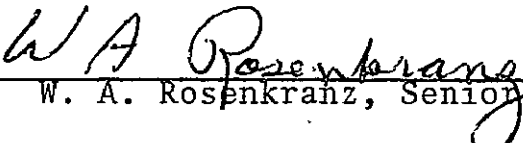
Houston, Texas

June 1975

LEC-6107


SCATTEROMETER RECEIVER DYNAMIC
RANGE/LINEARITY
(SPE-S193-005, S&AD)
Job Order 75-215

PREPARED BY




W. A. Rosenkranz, Senior Engineer

APPROVED BY



J. J. Carney, Supervisor
Exploratory Investigations Section



O. N. Brandt, Acting Manager
Earth Observations Exploratory Studies
Department

Prepared By

Lockheed Electronics Company, Inc.

For

EARTH OBSERVATIONS EXPLORATORY STUDIES DEPARTMENT

NATIONAL AERONAUTICS AND SPACE ADMINISTRATION
LYNDON B. JOHNSON SPACE CENTER
HOUSTON, TEXAS

June 1975

LEC-6107

ACKNOWLEDGMENTS

Special acknowledgment is due the deceased Dr. Dale E. Kaufman, a former Kansas State University Professor and Lockheed Employee, for his work on the rf link equation and radar cross-section calculation used in this report.

Acknowledgment is made to Donnie J. Pounds for his suggestions on the A/D converter. Kenneth P. Eckel is thanked for his programming support and additional time given to the project to help meet the project time schedule. The author also wishes to acknowledge special software for reading S-193 data tapes provided by Dr. A. C. Cook and Mike Lynch of the University of Kansas.

CONTENTS

Section		Page
1.0	<u>INTRODUCTION</u>	1
1.1	OBJECTIVE	1
1.2	DETAILED TASK DESCRIPTION AND APPROACH.	1
1.3	A DISCUSSION ON THE SCATTEROMETER DATA USED IN THIS INVESTIGATION.	2
2.0	<u>THE RF LINK EQUATION AND BACKSCATTER CALCULA- TION TECHNIQUES AS APPLIED TO SPE-005.</u>	4
2.1	INTRODUCTION.	4
2.2	THE RF LINK EQUATION.	4
2.3	THE S-193 SCATTEROMETER RECEIVER.	9
2.4	S-193 ANALOG-TO-DIGITAL CONVERTER CHARACTERISTICS AND INFLUENCE ON S-193 DATA OUTPUT.	14
3.0	<u>CALCULATION OF RADAR CROSS-SECTION</u>	30
4.0	<u>GROUND TRUTH AND SENSITIVITY ANALYSIS IN DETERMINING σ^o AND P_R</u>	39
4.1	INTRODUCTION.	39
4.2	GROUND TRUTH FOR THE GULF OF MEXICO	40
4.3	DETERMINATION OF SURFACE PROFILE.	44
4.4	ATMOSPHERIC LOSSES.	45
4.5	SL2/SL3 GROUND TRUTH.	45
5.0	<u>SKYLAB S-193 SCATTEROMETER INPUT/OUTPUT CHARACTERISTICS.</u>	50
5.1	INTRODUCTION.	50
5.2	I/O CURVES FOR ITNC SL2 DATA.	51
5.3	I/O CURVES OF SL2 ITC	55

Section		Page
6.0	<u>CONCLUSIONS</u>	58
7.0	<u>REFERENCES</u>	59
APPENDIX		
	SL2, SL3 SCATTEROMETER DATA.	A-1

TABLES

Table		Page
I	ERROR IN A/D CONVERTER OUTPUT.	17
II	SCATTEROMETER DATA AND VOLTAGES AS CALCULATED FROM MEASURED A/D CONVERTER OUTPUT	23
III	UNDERSTATED SCATTEROMETER DATA AND VOLTAGES AS CALCULATED FROM ANALOG OUTPUT DATA.	24
IV	COMPARISON OF σ° AND SCAT COUNTS THAT UNDERSTATES A/D CONVERTER OUTPUT	25
V	SCATTEROMETER DATA AND VOLTAGES CALCULATED FROM ANALOG OUTPUT DATA THAT OVERSTATES OUTPUT .	27
VI	COMPARISON OF σ° AND SCAT COUNTS CAUSED BY QUANTIZING MINIMUM ERROR.	28
VII	COMPARISON OF SCATTEROMETER DATA CAUSED BY INCREMENTAL DATA IN A/D CONVERTER.	29
VIII	SENSITIVITY OF σ° TO MEAN SQUARE SURFACE SLOPE/WIND VELOCITY ERROR.	46

FIGURES

Figure		Page
1	Geometry associated with S-193 radar target . . .	6
2	S-193 Scatterometer receiver block diagram. . .	10
3	A representative input/output curve for the S-193 Scatterometer receiver.	13
4	A/D converter characteristics	15
5	Scatterometer processor and relative voltage locations	21
6	Real part of the complex dielectric constant of pure, fresh and sea water vs frequency for 0°C and 20°C (ref. 15).	42
7	Imaginary part of the complex dielectric constant of pure, fresh and sea water vs frequency for a water temperature of 0°C and 20°C (ref. 15).	43
8	FOV for S-193 EREP Pass 8, time slice 6, wind speeds, sea height and wind direction, opera- ting mode ITNC.	48
9	FOV for S-193 EREP, Pass 20, time slice 4, wind speed, sea height, wind direction, operating mode ITC.	49
10	S-193 I/O characteristics, voltage into integrator (V^*) vs input power to antenna (P_R), EREP Pass 8, time slice 6, operating mode ITNC	53
11	S-193 theoretical backscatter vs measured back- scatter EREP Pass 8, time slice 6, operating mode ITNC	54
12	S-193 I/O characteristics, voltage into integrator (V^*), input power to antenna (P_R), EREP Pass 20, time slice 4, operating mode ITC.	56

Figure		Page
13	S-193 theoretical backscatter vs measured backscatter EREP Pass 20, time slice 4, operating mode ITC	57

1.0 INTRODUCTION

1.1 OBJECTIVE

~~This report summarizes~~ the results of an investigation aimed at determining the dynamic range and linearity of the S-193 scatterometer receiver from data acquired during Skylab missions 2 and 3. *412 74m*

1.2 DETAILED TASK DESCRIPTION AND APPROACH

The objectives of this task were accomplished by basically following the outline presented by the Sensor Performance Evaluation Implementation Plan (SPE-00413) (ref. 1). The data site (Gulf of Mexico) was selected for this investigation because it was one of the few sites where adequately detailed ground truth was available for backscatter (σ°) or radar cross-section calculations. This site also provided a range of σ° values that covered the expected dynamic range of the instrument. For many sites, neither a large variation in σ° values nor the needed ground truth was available.

From the ground truth of the data site selected, a target model amenable to calculating σ° was selected. The calculated σ° values were used in the rf link equation for the input power at the S-193 antenna (P_R) (ref. 2). The output of the S-193 scatterometer receiver was recorded as raw data (counts from the A/D converter) in the data product S062-1. This output versus the theoretical input power (P_R) was then graphically displayed, and the linearity and dynamic range determined.

Dynamic range was defined to be the range of input values that correspond to the A/D converter going from saturation to a point where noise level measurements were made. The degree of linearity of the S-193 scatterometer was defined two ways: (1) preflight versus measured data (input power/output voltage) and (2) theoretical backscatter (σ°) versus measured backscatter.

1.3 A DISCUSSION ON THE SCATTEROMETER DATA USED IN THIS INVESTIGATION

Two criteria were used in the selection of scatterometer data. First, the time slices of scatterometer data that were used showed a wide range of σ° values. All the scatterometer data was reviewed with respect to mode and maximum and minimum backscatter (σ°) values. These results are shown in tables A-I and A-II in the appendix. Second, for a given time slice of scatterometer data, an accompanying and complete set of ground truth was needed in order to calculate σ° . The dynamic range was anticipated to range from approximately -30 dB to +25 dB for σ° , based on preflight data (ref. 3).

Of the 41 time slices reviewed in the SL-2 scatterometer data, seven had σ° values greater than +15 dB and 17 had σ° values less than -25 dB. Only two time slices had σ° values greater than +15 dB and less than -25 dB. These two occurred over the Gulf of Mexico in passes five and eight.

There are four basic modes of operation of the S-193 scatterometer (ref. 4 and 5). They are: (1) in-track non-contiguous (ITNC), (2) in-track contiguous (ITC), (3) cross-track non-contiguous (CTNC) and (4) cross-track contiguous (CTC). The two previously noted time slices over the Gulf of Mexico occurred during ITNC operation of the scatterometer.

Two points of the SL-2 data reviewed showed saturation that occurred during two different CTC time slices. In showing saturation the maximum A/D converter output of 1023 counts was recorded. The reason for referencing the four different modes of operation (and the corresponding range of σ° values) is that for each individual mode of operation, different amplifier gains, filter and integrator characteristics within the S-193 scatterometer were used. As a result, each mode represents a somewhat slightly different subsystem. Ideally, all four modes of scatterometer operation should be reviewed for linearity and dynamic range. Adequate ground truth does not exist for all time slices in which a wider range of σ° values occur and therefore makes this impossible.

The S-193 scatterometer is discussed in section 1 (ref. 4 and 5). The remainder of this report is divided into five sections. Section 2 discusses the analytical approach to calculation of the S-193 power (P_R) received at the scatterometer antenna. Section 3 discusses the radar cross-section. Additionally, the scatterometer physical limitations are discussed with emphasis on the minimum and maximum values of σ° that can be measured. Section 4 elaborates on the ground truth available for the SPE-005 task and analyzes error or sensitivity in calculating σ° . Section 5 discusses pre-flight system input/output data, and calculated σ° values versus a measured output for both SL-2 and SL-3 data. Conclusions are developed in section 6.

2.0 THE RF LINK EQUATION AND BACKSCATTER CALCULATION TECHNIQUES AS APPLIED TO SPE-005

2.1 INTRODUCTION

This section presents analytical methods used in determining the power input (P_R) to the S-193 scatterometer antenna during the SL-2 and SL-3 missions. The power input is given by the rf link equation developed from the well-known radar equation (ref. 6).

2.2 THE RF LINK EQUATION

The power (P_R) collected by the radar receiving antenna is given in the following functional relation from the radar equation

$$P_R = P_T G_T \frac{1}{4\pi R^2 L_1} (\sigma) \frac{1}{4\pi R^2 L_2} \times \frac{G_R \lambda_o^2}{4\pi} \quad (1)$$

The various parameters of the above equation are defined as follows:

P_T = power radiated by the transmitting antenna in watts

G_T = gain of the transmitting antenna in the direction of the radar target

R = range between the radar and the radar target

L_1, L_2 = the path losses for transmission and reception, respectively, through the intervening medium

G_R = gain of the receiving antenna in the direction of the radar target

λ_o = transmitted radar signal wavelength

σ = radar cross-section or the effective area of the radar target reradiating energy back to the radar

In equation (1), σ represents the radar cross-section of the target. In this sense, the radar target is assumed to be infinitely small, whereas in fact, the radar target for the S-193 is modeled as a circular footprint on the earth with a diameter of 6 nautical miles. This is for the case in which the radar is pointed at nadir, $\theta = 0$ (see fig. 1). For angles of incidence other than $\theta = 0$, the footprint is approximately elliptical.

Kaufman has defined a normalized radar cross-section (σ°) for each incremental area in the circular 6 nautical mile S-193 target (ref. 2). Hence, an incremental area ΔA within the radar target contributes $\Delta\sigma$ to the radar target cross-section. A normalized radar cross-section for each incremental area of the S-193 radar target is defined as (ref. 2)

$$\sigma^\circ = \lim_{\Delta A \rightarrow 0} \frac{\Delta\sigma}{\Delta A} = \frac{d\sigma}{dA} \quad (2)$$

Also, the contribution ΔP_R to received power collected at the S-193 antenna as returned from the incremental area ΔA in the S-193 radar target is

$$\Delta P_R = \frac{P_T G_T G_R \lambda_o^2}{(4\pi)^3 \rho^4 L_1 L_2} \Delta\sigma \quad (3)$$

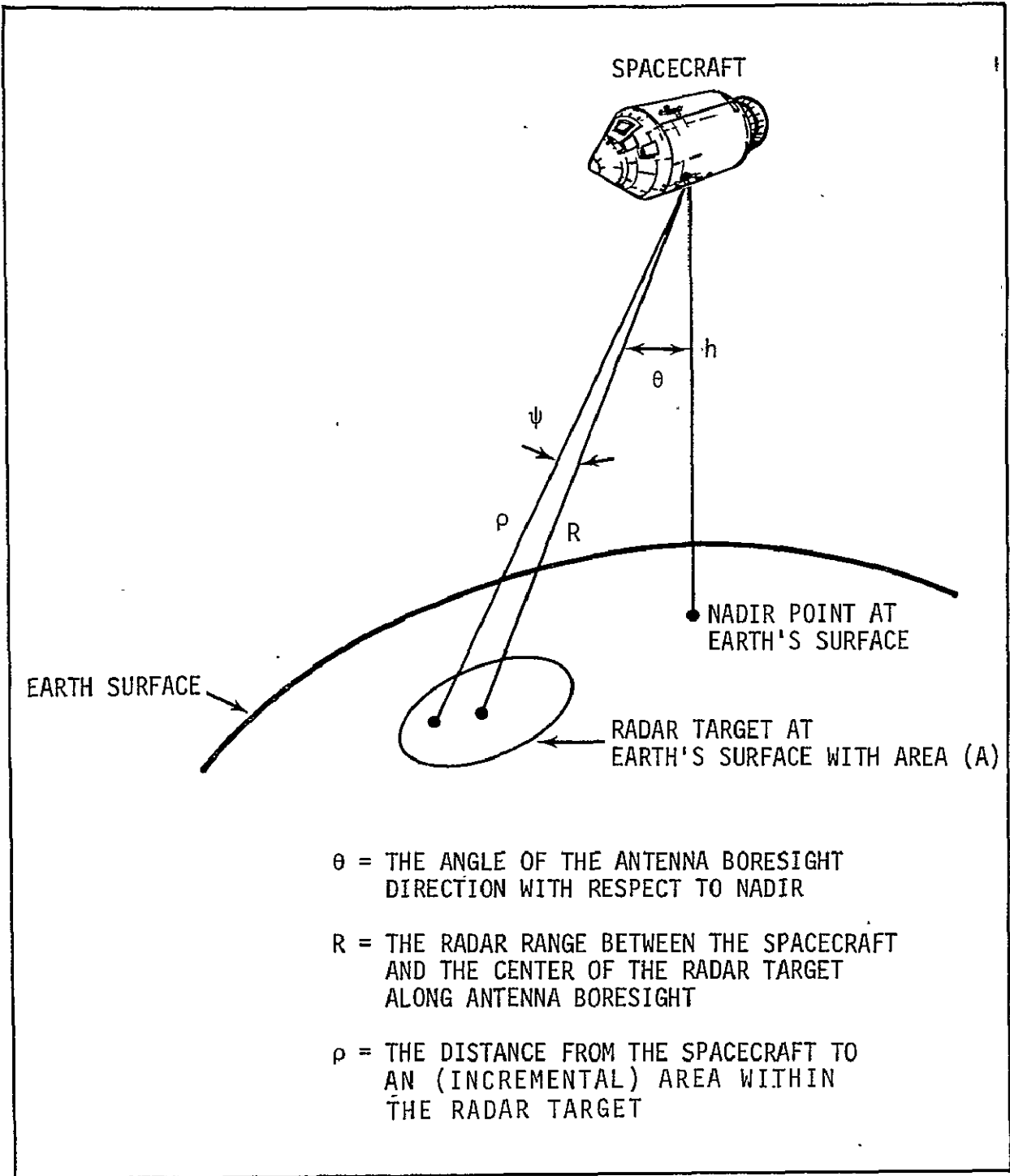


Figure 1. - Geometry associated with S-193 radar target.

The total power (P_R) collected at the S-193 antenna is then

$$\begin{aligned}
 P_R &= \frac{P_T \lambda_o^2}{(4\pi)^3} \int_A \frac{G_T G_R d\sigma}{\rho^4 L_1 L_2} \\
 &= \frac{P_T \lambda_o^2}{(4\pi)^3} \int_A \frac{G_T G_R \sigma^\circ}{\rho^4 L_1 L_2} dA \quad (4)
 \end{aligned}$$

with the integral being taken over the area A of the S-193 radar target.

In evaluating the above integral for the S-193 system, two approximations can be made:

- (1) σ° can be considered constant over A . In effect, σ° can be taken as an average value taken over the surface of the radar target.
- (2) With small relative error in the results, ρ can be considered as having a constant value $\rho = R$ over the radar target.

From equation (1), G_T and G_R are functions of the angle ψ (fig. 1) and vary across the radar target area A . Thus, integration over this area is necessary in computing P_R , the power returned to the S-193 antenna.

In addition, the transmitting and receiving antenna gains are defined as

$$G_T(\psi) = G_1 f_T(\psi)$$

$$G_T(\psi) = G_2 f_R(\psi)$$

$$G_1 = G_T(0)$$

$$G_2 = G_R(0)$$

$$G_0^2 = G_1 G_2 \quad (5)$$

where G_0^2 is the two-way antenna gain along the antenna boresight. If $f_T(\psi)$ and $f_R(\psi)$ are the one-way normalized antenna patterns associated with transmitting and receiving, equation (4) can be written in the form

$$P_R = \frac{P_R \lambda_0^2}{(4\pi)^3 R^4} \sigma^0 \frac{G_0^2}{L_1 L_2} \int f_T(\psi) f_R(\psi) dA \quad (6)$$

Equation (6) can be considered as the basic rf link equation because it predicts the return power from an S-193 radar target in terms of transmitted power, range, wavelength, atmospheric losses, antenna pattern and the normalized radar cross-section of the radar target. This is a key equation in the sensor performance evaluation of the S-193 scatterometer system.

The basic rf link equation has been further simplified.
Let

$$I_B = G_o^2 \int f_T(\psi) f_R(\psi) dA \quad (7)$$

The integral has been evaluated to give

$$I_B = I_C R^2 \sec \alpha \quad (8)$$

where I_C has been evaluated to give (ref. 7)

Transmitting polarization	Receiving polarization	I_C
V	V	6.778×10^4
H	H	7.146×10^4
V	V	6.745×10^4
H	H	6.745×10^4

Thus, equation (6) can be rewritten in the form

$$P_R = \frac{P_T \lambda_o^2 \sigma^o I_C \sec \alpha}{(4\pi)^3 R^2} \quad (9)$$

It is this form of the rf link equation that is used in calculating P_R , the power received at the S-193 scatterometer antenna.

2.3 THE S-193 SCATTEROMETER RECEIVER

The S-193 scatterometer receiver is shown in figure 2. Basically, there are three sections to this receiver: the rf, i.f., and scat processor sections. The rf and i.f. sections

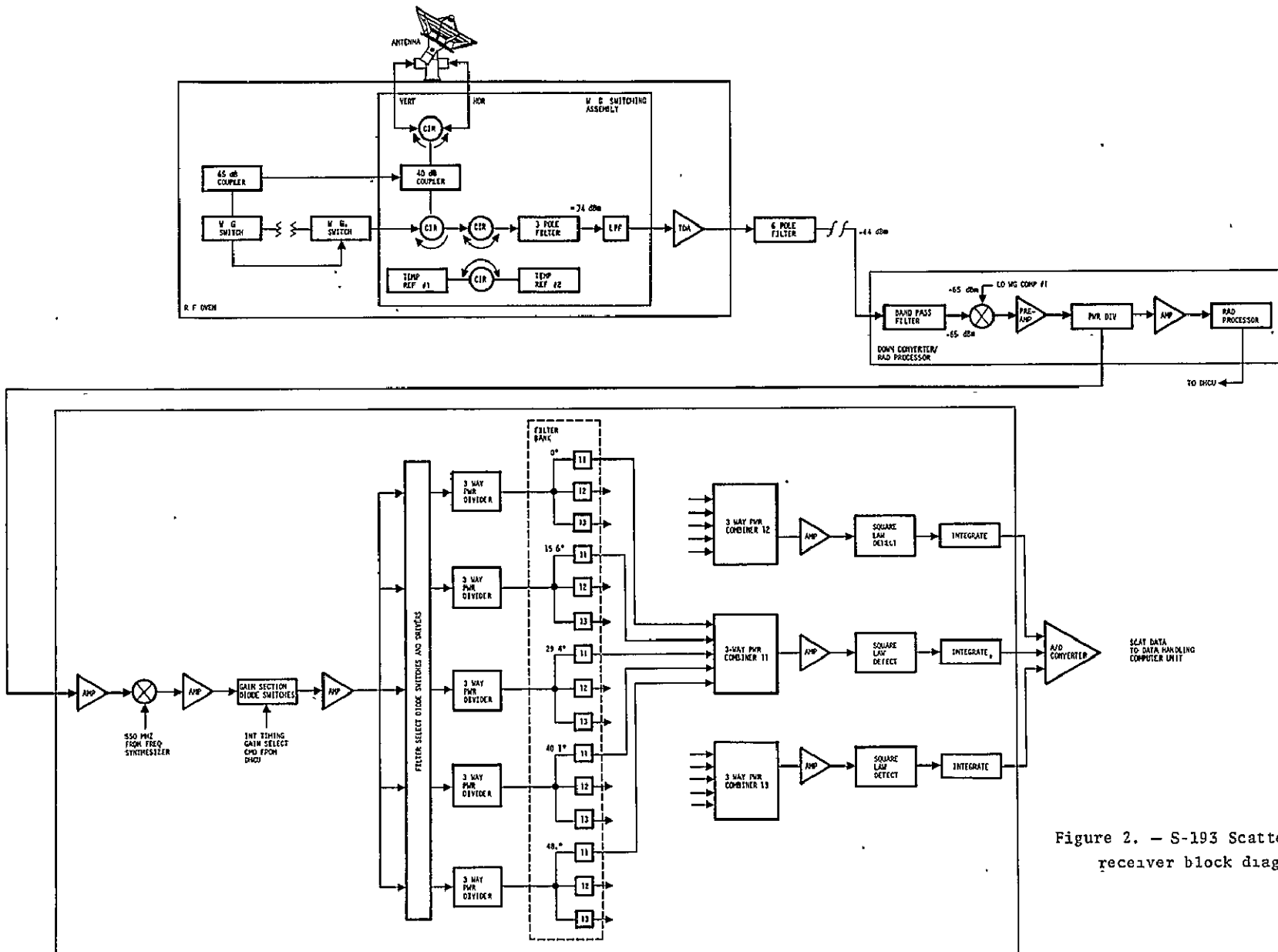


Figure 2. - S-193 Scatterometer receiver block diagram.

are discussed elsewhere (ref. 3, 4). The scat processor is discussed here to reemphasize that the signal path through the processor is variable and that certain elements in the processor limit this scatterometer performance.

A 50-MHz signal is fed into the gain selection diode switch block. The amplifier that follows provides a choice of 20, 30, 40 or 50 dB of gain through series resistive attenuation. The gain selection is determined by the strength of the returned signal. Then the signal is sent to one of five crystal filter banks. The filter bank selected is determined by the pitch angle of the spacecraft (0° , 15.6° , 29.4° , 40.1° , 48°). Within each filter bank are three filters, designated high center frequency (HCF), middle center frequency (MCF), and low center frequency (LCF). Following is a set of three five-way power combiners which individually receive a signal from the LCF, MCF or HCF filters. After amplification and detection, the signal (pulse train) is integrated according to source, (LCF, MCF or HCF filter). Additionally, depending upon which one of the five sets of three filters (according to pitch angle) the signal came from, the integration time is varied. The integration time varies depending on the mode of scat operation, i.e., ITNC, ITC, CTNC and CTC. After integration, the signal is passed to an A/D converter where the output is represented by counts in the S-193 scatterometer raw data (S062-1, A063). Thus, it can be seen that any radar return follows only one path through rf and i.f. sections but can follow any one of a variety of paths through the processor. This multiplicity of paths in the scatterometer processor is dependent upon the strength of the radar return (P_R) and pitch angle of the spacecraft. Thus, to completely discuss dynamic range and

linearity of the S-193 scatterometer receiver, all possible signal paths should be studied because each path represents a different instrument. However, this is not practical as will be explained shortly. Figure 3 shows a representative input/output curve for the S-193 scatterometer receiver.

After examining the SL-2 and SL-3 scatterometer data, it was observed that in many time slices, the data points would usually be clustered along one or two lines of the set of four. In fact, for SL-2 and SL-3 data, 40 percent of the data time slices operated about the High- or 2nd High-gain curves. Typically, the High- and 2nd High-gain curves were where most of the data points clustered when plotting V^* versus P_R .

A few time slices exist where the S-193 scatterometer backscatter data showed a sufficient range of values such that all four gain curves were utilized. A corresponding set of ground truth could be established whereby P_R could be calculated. (If P_R cannot be calculated, then the input to the scatterometer receiver cannot be ascertained by independent means and limitations exist in ascertaining the scatterometer receiver performance.) Methods of calculating radar backscatter σ° (radar cross-section) are discussed in section 3.

Where P_R represents the power into the receiver antenna, V^* represents the voltage into the integrator. A set of gain curves (High, 2nd High, Med Low, Low) for each of the HCF, MCF and LCF filters should be generated using measured data to completely characterize the scatterometer. However, the limitations of obtaining three sets of curves

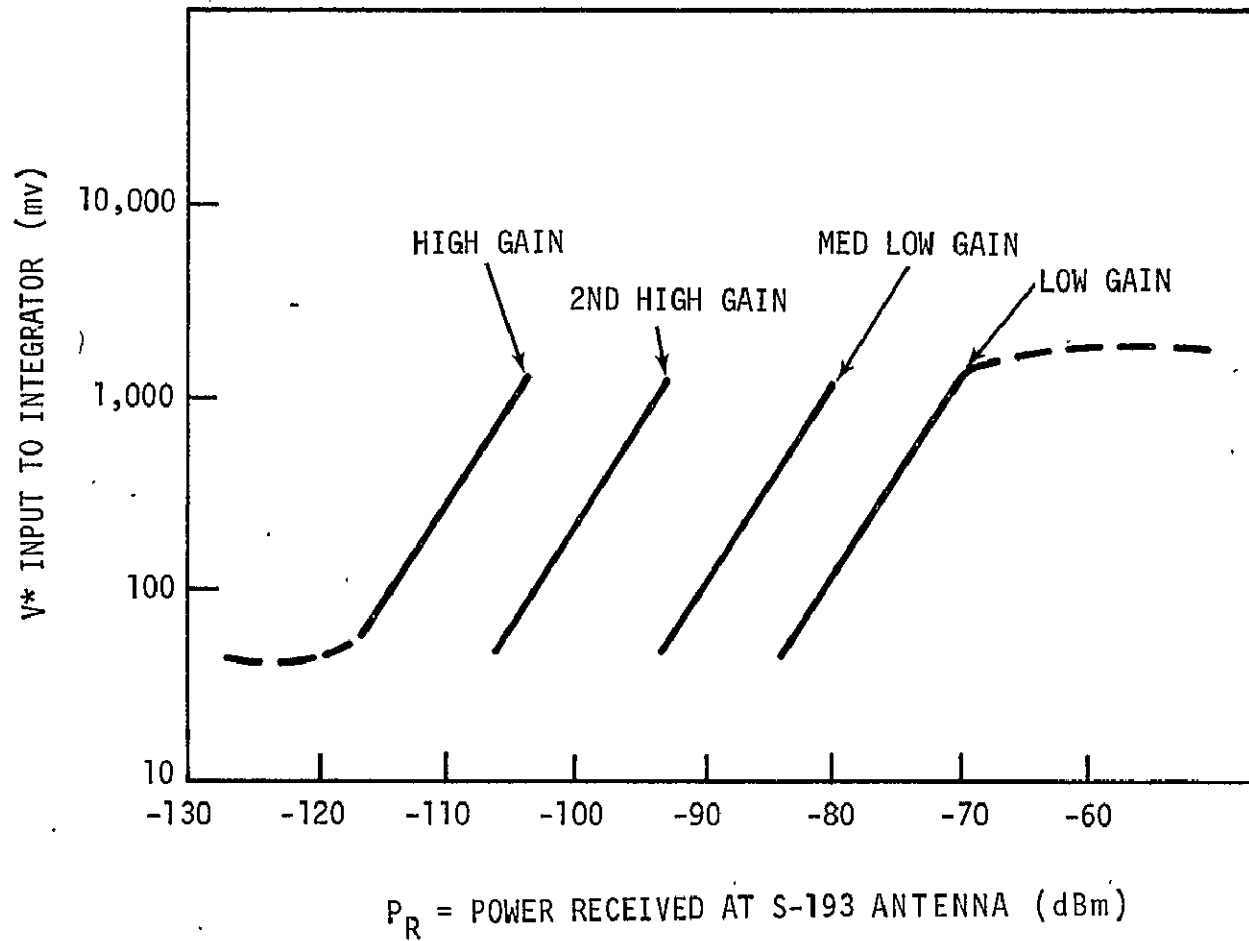


Figure 3. — A representative input/output curve for the S-193 Scatterometer receiver.

(one each for the LCF, MCF, HCF filters) are two-fold. First, the data is usually clustered about one local area on the graph.(i.e., not spread out so as to totally give the dynamic range) for any one time slice. Second, looking at all the time slices offers no solution since σ° and hence P_R cannot be evaluated because of lack of sufficient ground truth.

2.4 S-193 ANALOG-TO-DIGITAL CONVERTER CHARACTERISTICS AND INFLUENCE ON S-193 DATA OUTPUT

The analog-to-digital (A/D) converter in the scatterometer can influence the production data processing calculated value of σ° for low scatterometer backscatter signal levels.

At low signal levels the A/D converter granularity can misrepresent the true value of the measured signal to noise measurements relative to the noise measurements. From figure 4, it can be seen that for a change of 4.89×10^{-3} volts into the A/D converter, the output should change by one count.

The scatterometer signal into the converter includes signal and noise. Consider a scatterometer signal-plus-noise of V_S volts. Let the voltage (V_S) satisfy the following relationship:

$$V_1 < V_S < V_3 \quad (10)$$

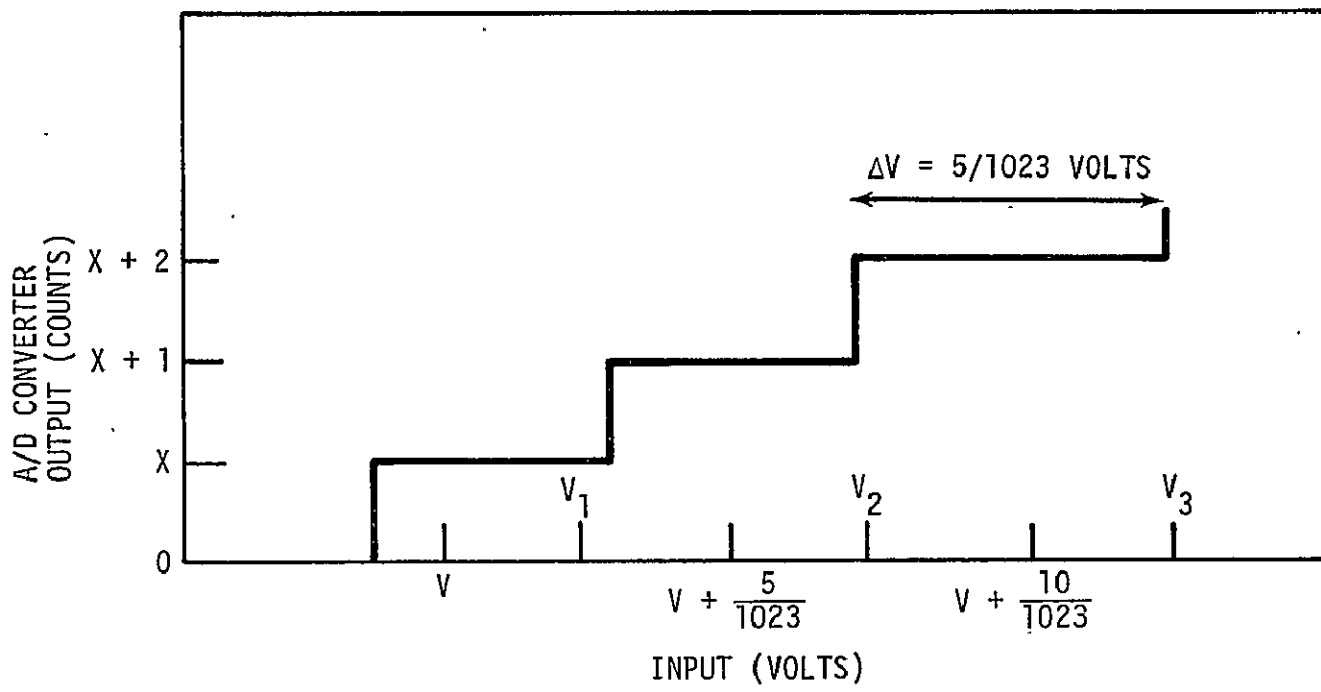


Figure 4. - A/D converter characteristics.

For this range of values of V_S , the output is $X + 1$ or $X + 2$ counts. Consider the case where the signal-plus-noise voltage V_{S+N} and the noise voltage V_N have the following values:

$$V_1 < V_N < V_2 \quad \text{and} \quad V_2 < V_{S+N} < V_3 \quad (11)$$

The corresponding outputs would be $X + 1$ counts for noise and $X + 2$ counts for signal-plus-noise. If equation (11) were rewritten as:

$$V_1 \leq V_N \leq V_2 \quad \text{and} \quad V_2 \leq V_{S+N} \leq V_3 \quad (12)$$

then the difference in output counts could vary from "0" to "2". For a difference in signal-plus-noise output and noise output of n counts, the maximum output approaches $(n + 1)$ counts and the minimum output approaches $(n - 1)$.

Hence the actual output of the A/D converter can be increased or decreased by one count because of the granularity of the A/D converter. For a large signal-plus-noise-to-noise ratio where n is large, this effect is of little concern. For the case where the signal-plus-noise-to-noise is small, then the overstatement or understatement of the output by one count gains importance. For insight into the relative effect of understating or overstating the output by one count, with respect to n counts difference between signal-plus-noise and noise, see table I.

Depending upon whether the output is overstated or understated, the following equations are used to express the relative discrepancy. This discrepancy is expressed in decibels.

TABLE I. - ERROR IN A/D CONVERTER OUTPUT

$\Delta C=n$	ΔC in millivolts	$10 \log \left(\frac{n}{n-1} \right)$ dB (a)	$10 \log \left(\frac{n+1}{n} \right)$ dB (b)
1	4.888	∞	3.01
2	9.775	3.01	1.76
3	14.663	1.76	1.25
4	19.550	1.25	.97
5	24.438	.97	.79
6	29.326	.79	.67
7	34.213	.67	.58
8	39.101	.58	.51
9	43.988	.51	.46
10	48.876	.46	.41
11	53.763	.41	.38
12	58.651	.38	.35
13	63.539	.35	.32
14	68.426	.32	.30
15	73.314	.30	.28
16	78.201	.28	.26
17	83.089	.26	.25
18	87.977	.25	.23

^aRelative understatement.

^bRelative overstatement.

$$\begin{aligned} \text{relative understatement} &= 10 \log \left(\frac{n}{n-1} \right) \\ \text{relative overstatement} &= 10 \log \left(\frac{n+1}{n} \right) \end{aligned} \quad (13)$$

where n = difference in output counts for signal-plus-noise ($V_S + N$) and noise (V_N).

For the case of understating the output, the relative effect is greater than that of overstating the output. Note that as n increases, the relative effect of misstating the output by one count decreases rapidly.

The accuracy of determination of σ° is affected directly for low signal level. Table I shows the difference in counts (ΔC) or (millivolts) for maximum and minimum errors in dB.

It should be noted that the output counts from the converter for noise and those for signal-plus-noise do not represent proportionate voltage in the earlier stages of the receiver. Relative backscatter noise voltages (V_N'') and signal voltages (V_S'') are given in the S-193 data product S062-15. These voltages are scaled from the actual measured output counts to account for differences in amplifier gain, integrator integration times, and integrator time constants used for scatterometer signal-plus-noise and noise measurements. The relationship between counts and relative backscatter voltages is given in equation (14) and figure 5. The effect of V_S' and V_N' upon the calculations of σ° is shown in equation (14). Equation (14) represents the method used to calculate σ° for the S-193 data.

$$\sigma^{\circ} = \frac{(4\pi)^3 R^4}{\lambda^2} (L_1 L_2) \frac{P_R}{P_T} \times \frac{1}{I_C \sec \alpha}$$

where

$$\frac{P_R}{P_T} = \frac{K_C}{K_R K_T} \left[\frac{(IT)_C}{(IT)_S} \times \frac{(TC)_S}{(TC)_C} \times \frac{F_C}{F_S} \times \frac{G_C}{G_S} \right] \times AC(DF) \times \left\{ \frac{V'_S - V'_N \times \left[\frac{(IT)_S}{(IT)_N} \times \frac{(TC)_N}{(TC)_S} \times \frac{F_S}{F_N} \times \frac{G_S}{G_N} \right]}{V'_C} \right\} \quad (14)$$

K_C, K_R, K_T = constants related to internal calibrate, receive, and transmit path losses in the scatterometer rf section

F_C, F_S, F_N = calibration, signal, and noise filter constants

The subscripts S, N, and C in equation (15) refer to scatterometer signal-plus-noise, noise, and internal calibration measurements respectively.

$$V_S = \frac{5}{1023} \times \text{Counts}$$

$$V_N = \frac{5}{1023} \times \text{Counts}$$

$$V_C = \frac{5}{1023} \times \text{Counts}$$

$$V'_S = V_S - q \times (IT)_S / (TC)_S - (IT)_S \times \text{drift}$$

$$V'_N = V_N - q \times (IT)_N / (TC)_N - (IT)_N \times \text{drift}$$

$$V_C' = V_C - q \times (IT)_C / (TC)_C - (IT)_C \times \text{drift}$$

$$V_S' = (V_S' / G_S) \times (TC)_S / (IT)_S$$

$$V_N' = (V_N' / G_N) \times (TC)_N / (IT)_N$$

$$V_C' = (V_C' / G_C) \times (TC)_C / (IT)_C$$

$$V_S' = V_S^* \times \frac{IT_S}{TC_S}$$

$$V_N' = V_N^* \times \frac{IT_N}{TC_N}$$

$$V_C' = V_C^* \times \frac{IT_C}{TC_C} \tag{15}$$

V_S, V_N, V_C = signal-plus-noise, noise, and internal calibration voltages input to the A/D converter.

V_S', V_N', V_C' = corrected signal-plus-noise, noise and internal calibration voltages at the integrator output. The correction is for integrator drift.

V_S'', V_N'', V_C'' = signal-plus-noise, noise, internal calibration voltages into the scatterometer processor multiple gain amplifier

IT, TC = integrator integration time and time constant values

q = integrator drift

drift = integrator drift correction

G = amplifier gain

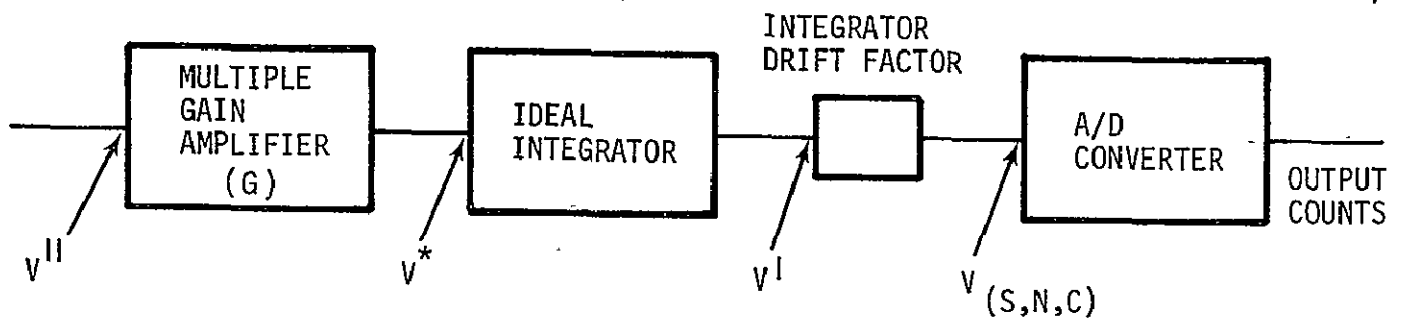


Figure 5. - Scatterometer processor, relative voltage locations.

To relate the effect of understating or overstating the output of the A/D converter to these voltages, table II and subsequent analysis are used. These data for EREP pass eight, time slice six, utilize data products S062-1, S062-15, and S062-16. This is an ITNC mode of operation. The purpose of this analysis is to show that even though more than one or two counts difference between signal-plus-noise and noise measurements may exist, the effect of integration times, time constants and gains on voltages that are subsequently converted to counts may be misleading. That is, because of the difference between small signal-plus-noise to noise measurements, A/D converter granularity-induced errors may result in an erroneous value of calculated σ° which, in net effect, limits the lower extent of the effective dynamic range that the scatterometer data user can confidently utilize.

Note understating the A/D converter output for each of the data points in table II. The difference in output counts (n) from the A/D converter for scatterometer signal-plus-noise and scatterometer noise as presented in the raw data is n counts, whereas for this case it should have been (n - 1) counts. A similar set of parameters is computed for table IV. The variation is assumed to be in scatterometer signal-plus-noise while the scatterometer noise and calibration output values remain constant.

Thus from table IV, the change in scatterometer signal-plus-noise counts by a minus one count for σ° values less than -31 dB changes the values of σ° drastically. Since the values of σ° below -31 dB are subject to the limitations of the A/D converter, these σ° values should be used with

TABLE II. - SCATTEROMETER DATA AND VOLTAGES AS CALCULATED
FROM MEASURED A/D CONVERTER OUTPUT

Data pt	Measured noise counts output	Measured scat counts output	σ° (dB) PDP	V_S (volts) (calculated)	V_N (volts) (calculated)	V_S (volts) (calculated)	V_N (volts) (calculated)
1	34	41	-36.47	.0409	.0374	.17348	.1422696
2	34	42	-35.24	.0421	.0374	.17857	.1422696
3	34	46	-32.26	.0467	.0374	.19808	.1422696
4	34	49	-31.14	.0502	.0374	.21292	.1422696
5	34	64	-27.21	.0674	.0374	.28587	.1422696
6	34	94	-24.11	.1020	.0374	.43263	.1422696

TABLE III. - UNDERSTATED SCATTEROMETER DATA AND VOLTAGES AS CALCULATED
FROM ANALOG OUTPUT DATA

Data pt	Measured noise counts output	Modified scat counts output	Modified V'_S (calculated)	Modified V'_N (calculated)	Modified V''_S (calculated)	Modified V''_N (calculated)	Modified σ° (dB)
1	34	40	.1688098	.1422696	.039821	.0374	a
2	34	41	.173708	.1422696	.040900	.0374	-47.45
3	34	45	.193258	.1422696	.045564	.0374	-33.22
4	34	48	.207921	.1422696	.049021	.0374	-31.72
5	34	63	.281235	.1422696	.0663062	.0374	-27.40
6	34	93	.454545	.1422696	.107167	.0374	-24.19

^aBy decreasing the value of scat counts by one, the value of P_R/P_T became negative so that the value of σ° in dB cannot be expressed.

TABLE IV. - COMPARISON OF σ° AND SCAT COUNTS THAT
UNDERSTATES A/D CONVERTER OUTPUT

Data pt	Measured scat counts output	Modified scat counts output due to quantizing error	Measured noise counts output	Measured σ° dB	Modified σ° dB	$\Delta\sigma^\circ$ dB
1	41	40	34	-36.47	a	a
2	42	41	34	-35.24	-47.45	-12.21
3	46	45	34	-32.26	-33.22	-0.96
4	49	48	34	-31.14	-31.72	-0.58
5	64	63	34	-27.21	-27.40	-0.19
6	94	93	34	-24.11	-24.19	-0.08

^aBy decreasing the value of scat counts by one, the value of P_R/P_T became negative so that the value of σ° in dB cannot be expressed.

caution. Again although the measured difference in noise counts to signal-plus-noise counts for data points number one through four was seven to 14 counts, a variation in the scatterometer signal-plus-noise by one count caused resulting variations in σ° of one to twelve dB in the negative direction.

The error caused by an increase of one in the count difference between the signal-plus-noise and noise outputs from the A/D converter is next considered. This corresponds to overstating the output as given in table I and discussed earlier. The results are given in table V.

The output counts and scatterometer data from tables III and V are shown in table VII. This allows for a quick comparison of values of the two possible A/D converter outputs generated by the quantizing of the A/D converter signal.

In conclusion, there must be at least 14 counts difference in the output of the A/D converter for signal-plus-noise and noise to ensure data quality. Thus σ° values below about -31 dB should be used with caution.

TABLE V. - SCATTEROMETER DATA AND VOLTAGES CALCULATED FROM
ANALOG OUTPUT DATA THAT OVERSTATES OUTPUT

Data pt	Noise counts	Modified scat counts	Modified V_S	V_N	Modified V_S	V_N	Modified σ°
1	34	42	.178596	.1422696	.0421072	.0374	-24.0
2	34	43	.183483	.1422696	.0432594	.0374	-32.36
3	34	47	.203034	.1422696	.0472252	.0374	-31.48
4	34	50	.217696	.1422696	.0513257	.0374	-30.63
5	34	65	.291010	.1422696	.0686109	.0374	-27.03
6	34	95	.437638	.1422696	.1031811	.0374	-24.03

TABLE VI. — COMPARISON OF σ° AND SCAT COUNTS CAUSED BY
 QUANTIZING MINIMUM ERROR

Data pt	Measured scat counts outputs	Modified scat counts output due to quantizing minimum error	Measured noise counts output	Measured σ° dB	Modified σ° dB	$\Delta\sigma^\circ$ dB
1	41	42	34	-36.47	-24.00	+12.47
2	42	43	34	-35.24	-32.36	+2.92
3	46	47	34	-32.26	-31.48	+0.78
4	49	50	34	-31.14	-30.63	+0.51
5	64	65	34	-27.21	-27.03	+0.18
6	94	95	34	-24.11	-24.03	+0.08

TABLE VII. - A COMPARISON OF SCATTEROMETER DATA CAUSED BY
INCREMENTAL CHANGES IN A/D CONVERTER

Data pt	Scat output σ° counts (S_c)		Modified scat counts and σ° for understatement of A/D converter output (S_c-1)		Modified scat counts and σ° for overstatement of A/D converter output (S_c+1)	
	Counts	σ° (dB)	Counts	σ° (dB)	Counts	σ° (dB)
1	41	-36.47	40	a	42	-24.00
2	42	-35.24	41	-47.45	43	-32.36
3	46	-32.26	45	-33.22	47	-31.48
4	49	-31.26	48	-31.72	50	-30.63
5	64	-27.21	63	-27.40	65	-27.03
6	94	-24.11	93	-24.19	95	-24.03

^aBy decreasing the value of scat counts by one, the value of P_R/P_T becomes negative. Thus the value of σ° in decibels cannot be expressed.

3.0 CALCULATION OF RADAR CROSS-SECTION

The radar cross-section σ (or backscatter) of a target is defined as a quantitative measure of the ratio of power density in the vector signal, scattered in the direction of the receiver, to the power density of the radar wave incident upon the target (ref. 6). The normalized radar cross section is defined as (ref. 2)

$$\sigma^{\circ} = 4\pi R^2 \frac{\text{Average Power Scattered Back to Radar}}{\text{Power Incident at the Surface}} \quad (16)$$

According to Kaufman, "No satisfactory general theory for predicting radar backscatter from terrestrial surfaces exists. Such surfaces, even one as simple as the sea, cannot be described accurately in mathematical terms. Also, most schemes for the theoretical evaluation of σ° require approximations that constrain the result to a limited subset of terrestrial surfaces. Nonetheless, for simple surfaces, theory can provide reasonable estimates or bounds for the radar cross section" (ref. 2).

The mathematical models available for calculating σ° are of three types. They are: (1) semi-empirical models, (2) geometrical models, and (3) statistical models, all of which are discussed in depth elsewhere (ref. 2 and 8). For the SPE-005 task, only the results derived from statistical models will be used and are given later without derivation (ref. 2). Only normalized cross section σ° is considered here. These statistical models have the following constraints:

1. The distance from the radar to the radar target is assumed great enough so that the electromagnetic

wave incident upon the radar target or rough surface can be considered a plane wave. Correspondingly, the reflected wave from the target to the radar receiver can also be considered a plane wave at the receiver.

2. The radar return from subsurface features is not predicted.
3. The radar target is considerably larger than the transmitted radar signal wavelength.
4. The radar target has isotropic statistical properties which are time-invariant.
5. The dielectric constant at the surface is assumed constant over the radar target.

For any rough surface, the measured and calculated value of the normalized radar cross-section (σ^0) is dependent upon several factors:

1. The wavelength of the transmitted radar signal.
2. The surface profile of the scattering target.
3. The complex dielectric constant $\epsilon_r = \epsilon'_r - j\epsilon''_r$.
4. The angle at which the incident wave strikes the rough surface.
5. Polarization of the incident wave.

For a smooth surface without any roughness, an incident wave would be reflected according to Snell's Law. The amplitude of the reflected wave would be equal to the incident wave times the proper polarization dependent Fresnel reflection coefficient.

The Fresnel reflection coefficients are given as (ref. 2 and 9)

$$R_H = \frac{\epsilon_r \cos\alpha - (\epsilon_r - \sin^2\alpha)^{1/2}}{\epsilon_r \cos\alpha + (\epsilon_r - \sin^2\alpha)^{1/2}} \quad (17)$$

$$R_V = \frac{\cos\alpha - (\epsilon_r - \sin^2\alpha)^{1/2}}{\cos\alpha + (\epsilon_r - \sin^2\alpha)^{1/2}} \quad (18)$$

where α is the angle of incidence, i.e., the angle between the incident wave and the normal to the surface at the point of incidence. ϵ_r is the relative electric permittivity of the surface. The H and V subscripts indicate horizontal and vertical polarization of the incident wave.

For a rough surface, statistical models, which describe the surface, customarily treat the surface height variations about a mean planar surface as a random variable. Associated with the random variable or surface height are a set of statistical parameters, i.e., surface height distribution function, correlation function, etc. An rms surface height (σ) is associated with the distribution function and a correlation length (ℓ) is associated with the correlation function. For a Gaussian distribution function, a mean square slope can be defined as follows (ref. 2).

$$S^2 = 2\sigma^2/\ell^2 \quad (19)$$

All the statistical models used in this report are based upon a Gaussian surface height distribution. In the case of

a smooth surface, the power component of the scattered wave is called the "coherent" component because a constant, easily predictable, scattered field amplitude and phase pattern exist at a given point for a given surface position.. This is specular reflection. As the surface roughness increases, the scattered wave is reflected not in a manner described by equation 17 and 18, but instead, in a much more complex manner. This scattering is termed both specular and non-specular, and the scattered power component in the non-specular direction is termed "incoherent." For the incoherent scattered wave, the phase is a random variable. As the roughness increases, the incoherent component dominates over the coherent component. For σ (the rms surface height) greater than a wavelength, the coherent component is unrecognizable.

Essentially, all natural surfaces have what is called composite roughness (ref. 2). Generally, this is a "very rough" surface profile termed large scale roughness along with a "slightly rough" surface profile termed small scale roughness. For large scale roughness $\sigma \gg \lambda$ and for small scale roughness $\sigma \ll \lambda$. Both types of roughness scatter only incoherently since the coherent component of the scattered wave is suppressed by the large scale roughness. For example, mountains and valleys would represent large scale roughness whereas foliage on these mountains and valleys would represent the small scale roughness. Similarly, for the ocean, gravity waves would represent large scale roughness, and capillary waves imposed on the gravity waves would represent small scale roughness.

When the incident wave is near the normal to the mean planar surface so that the angle of incidence (α) is, almost

zero, the radar backscatter is primarily due to large scale roughness (ref. 2). For angles of incidence greater than 30° , small scale roughness is the dominant influence on radar backscattering (ref. 2 and 9).

The statistical models used in calculating the normalized radar cross-section for purposes of evaluating the S-193 scatterometer receiver performance are given here (ref. 2). Three requirements listed by Kaufman are:

- (1) $\ell \ll A$, i.e., the correlation length of the surface roughness is much less than the dimension of the illuminated area.
- (2) The surface slopes S , are less than .3 in magnitude.
- (3) $|\epsilon_r| > 1.4$

A composite model is used so that individual equations for large scale roughness and small scale roughness are combined to give a resultant σ° . From the equation (19) for large scale roughness, there exists the following:

- (1) σ_{LS} (large scale rms height) $\gg \lambda$
- (2) S_{LS} , ℓ_{LS} ; large scale rms slope
- (3) ℓ_{LS} ; correlation length

and for small scale roughness:

- (1) $\sigma_{SS} \ll 1$
- (2) $S_{SS} \ll 1$

The equations, which calculate the component of backscatter due to large scale roughness, express σ° in terms of the mean square slope and not rms height (σ_{LS}) or correlation length (ℓ_{LS}).

The backscatter component, calculated by the equations related to small scale roughness, expresses σ_{SS}° in terms of the rms height (σ_{SS}) and correlation length (ℓ_{SS}) and not the mean square slope (S_{SS}^2). Therefore, even though there is a mean square slope, rms height, and correlation length associated both with large and small scale roughness, the use of subscripts will be dropped. However, S^2 refers to the mean square slope for large scale roughness, and σ and ℓ refers to rms height and correlation length for small scale roughness in the following equations. The normalized radar backscatter that is derived from the two different roughness models will be appropriately subscripted.

For large scale roughness, σ_{LS}° is expressed as (ref. 2 and 9).

$$\sigma_{LS}^\circ = \frac{\sec^4 \alpha}{2s^2} |R(o)|^2 \exp \left(\frac{-\tan^2 \alpha}{2s^2} \right) \quad (20)$$

where

$$|R(o)| = \left| \frac{1 - \sqrt{\epsilon_r}}{1 + \sqrt{\epsilon_r}} \right|$$

and is dominant for small α . Note that the effect of polarization is not included here. $R(o)$ comes from the

Fresnel reflection coefficients for small α and ϵ_r is the complex permittivity for the particular radar target in question. For small angles of incidence, Kaufman differentiates between horizontal and vertical polarization in his expressions for large scale normalized radar backscatter (ref. 2).

For horizontal transmit and receive polarization and large scale roughness, the backscatter is given by

$$\sigma_{\text{HHLS}}^{\circ} = \frac{1}{2s^2} \left| R_h \sec^2 \alpha + (R_h - 1) K_1 \tan \alpha \right|^2 \exp \left(\frac{\tan^2 \alpha}{2s^2} \right)$$

where

$$R_h = \frac{\epsilon_r \cos \alpha - (\epsilon_r - \sin^2 \alpha)^{1/2}}{\epsilon_r \cos \alpha + (\epsilon_r - \sin^2 \alpha)^{1/2}}$$

$$K_1 = \left[1 - \frac{\cos \alpha}{(\epsilon_r - \sin^2 \alpha)^{1/2}} \right] \tan \alpha \quad (21)$$

For vertical transmit and receive polarization and large scale roughness, the backscatter is given by

$$\sigma_{\text{VVLS}}^{\circ} = \frac{1}{2s^2} \left| R_v \sec^2 \alpha + (R_v + 1) K_2 \tan \alpha \right|^2 \exp \left(\frac{\tan^2 \alpha}{2s^2} \right)$$

where

$$R_V = \frac{\cos \alpha - (\epsilon_r - \sin^2 \alpha)^{1/2}}{\cos \alpha + (\epsilon_r - \sin^2 \alpha)^{1/2}}$$

$$K_2 = \frac{\epsilon_r(1 - \epsilon_r) \sin \alpha}{(\epsilon_r - \sin^2 \alpha) \left[\epsilon_r \cos \alpha + (\epsilon_r - \sin^2 \alpha)^{1/2} \right]} \quad (22)$$

For small scale roughness, the normalized radar backscatter is given by

$$\sigma_{\text{HHSS}}^{\circ} = 4K^2 \sigma^2 \ell^2 |\alpha_{\text{hh}}|^2 (\cos^4 \alpha) \exp(-k^2 \ell^2 \sin^2 \alpha) \quad (23)$$

where

$$\alpha_{\text{hh}} = \frac{\epsilon_r - 1}{\left[\cos \alpha + (\epsilon_r - \sin^2 \alpha)^{1/2} \right]^2}$$

$$\sigma_{\text{VVSS}}^{\circ} = 4k^2 \sigma^2 \ell^2 |\alpha_{\text{vv}}|^2 (\cos^4 \alpha) \exp(-k^2 \ell^2 \sin^2 \alpha)$$

where

$$\alpha_{\text{vv}} = \frac{(\epsilon_r - 1) \left[(\epsilon_r - 1) \sin^2 \alpha + \epsilon_r \right]}{\left[\epsilon_r \cos \alpha + (\epsilon_r - \sin^2 \alpha)^{1/2} \right]^2} \quad (24)$$

and the condition $(2\pi\sigma/\lambda < 1)$ is applicable. Kaufman has accounted for polarization dependence here.

The composite normalized radar cross-section is given as

$$\sigma^{\circ}_{\text{TOTAL}} = \sigma^{\circ}_{\text{SS}} + \sigma^{\circ}_{\text{LS}} \quad (25)$$

and

$$\sigma^{\circ}_{\text{TOTAL}} (\text{dB}) = 10 \log_{10}(\sigma^{\circ}_{\text{TOTAL}}) \quad (26)$$

Note that $\sigma^{\circ}_{\text{TOTAL}}$ depends upon the particular polarization of $\sigma^{\circ}_{\text{SS}}$ and $\sigma^{\circ}_{\text{LS}}$.

Kaufman has an expression for the case where the cross-polarized normalized radar backscatter is desired. It is (ref. 2)

$$\sigma_{\text{VH}} = \sigma_{\text{HV}} = \frac{\lambda^2}{8\pi^2 \sigma^2 \sin 2\alpha} |R_{\text{H}} + R_{\text{V}}|^2 \exp\left(\frac{-\tan^2 \alpha}{2s^2}\right) \quad (27)$$

4.0 GROUND TRUTH AND A SENSITIVITY ANALYSIS
IN DETERMINING σ° AND P_R

4.1 INTRODUCTION

Basically, the ground truth used in evaluating the S-193 scatterometer for SL2/SL3 is available from four sources. They are:

- (1) Radiosonde data
- (2) National Oceanographic and Atmospheric Administration data
- (3) JSC aircraft flight data
- (4) Various independent studies of related ground scenes.

There are basic limitations in obtaining the necessary ground truth for calculating σ° and they are:

- (1) Wind speeds and temperature data recorded at times and/or locations other than that actually covered by an S-193 pass.

This is the case for wind velocity measurements over the ocean. This presents problems in estimating S^2 , σ^2 , and ℓ^2 .

- (2) Geologic surface information not thoroughly mapped, as an example, the Great Salt Lake Desert.

The four basic parameters to be determined from ground truth are S^2 , σ , ℓ and ϵ_r .

4.2 GROUND TRUTH FOR THE GULF OF MEXICO

The first quantity to be determined here was ϵ_r , the complex relative permittivity for the ocean water at the surface.

The value of ϵ_r is needed in calculating R_H , R_V , $R(O)$, K_1 , K_2 , α_{hh} and α_{vv} as given in the preceding section. Data has been taken for evaluating the relative permittivity (ϵ_r) of sea water. Since the incident radar beam is reflected in a manner almost entirely dependent upon the properties of the sea surface (or ground surface), the equations predicting σ° are based upon surface properties. For example, certain properties, such as sea temperature, vary with depth. The value of ϵ_r at the surface is dependent upon temperature, salinity, conductivity and frequency. As for frequency dependence, it can be seen from figures 6 and 7 that the real part of ϵ_r varies rapidly with frequency, and the imaginary part of ϵ_r is relatively constant for frequency variations between 10 GHz and 30 GHz. The complex permittivity was calculated from existing ground truth and established data that provide parameters necessary for computing ϵ_r .

From Paris, the real (ϵ_r') and imaginary (ϵ_r'') parts for the complex permittivity of the sea surface are determined from the following equations (ref. 10).

$$\begin{aligned}\epsilon_r &= \epsilon_r' - j\epsilon_r'' \\ \epsilon_r' &= \epsilon_\infty + (\epsilon_s - \epsilon_\infty)/(1 + \omega^2\tau^2) \\ \epsilon_r'' &= \omega(\epsilon_s - \epsilon_\infty)/(1 - \omega^2\tau^2) + \sigma_i/\omega\epsilon_0\end{aligned}\quad (28)$$

where ω = radian frequency of the incident energy

σ_i = ionic conductivity

τ = relaxation time

ϵ_∞ = a constant

$\epsilon_0 = \frac{10^{-9}}{36\pi}$ Farads

ϵ_s = static relative permittivity

The values of ϵ_s , τ , σ_i are determinable if the temperature of the water as the surface is known (ref. 10). From Pierson (ref. 11) and National Oceanographic and Atmospheric Administration (NOAA) data the temperature of the water at the surface in the Gulf of Mexico was about 27° C for Pass 8 (SL-2) and a value for salinity of 35 percent was used in obtaining equation (29) (ref. 10 and 11).

$$\epsilon_r = 47.63 - j36.39 \quad (29)$$

An interesting and important fact is that rain, over a given area of salt water, will reduce salinity at the surface for up to two hours after the rainfall. Correspondingly, the value of ϵ_r will change (ref. 11). NOAA reports no rainfall just prior to SL-2 Pass 8 over the Gulf of Mexico. Hence, for purposes of calculating σ° , which requires a knowledge of ϵ_r over the radar site, it has been assumed that the salinity and water surface temperature have remained essentially constant for this data-take. Therefore, the value of ϵ_r is assumed constant for the SL-2 Pass 8 over the Gulf of Mexico.

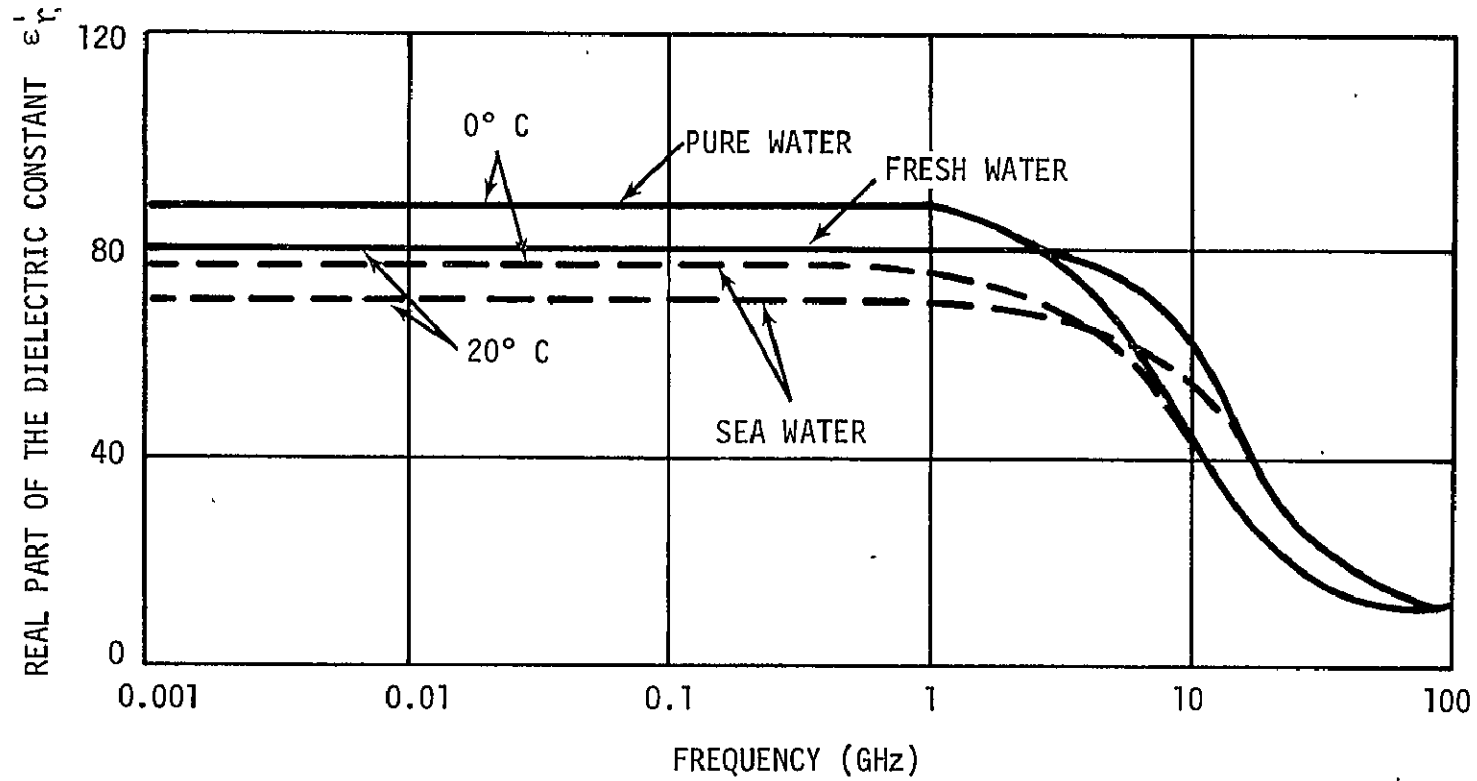


Figure 6. — Real part of the complex dielectric constant of pure, fresh and sea water vs frequency for 0° C and 20° C (ref. 15).

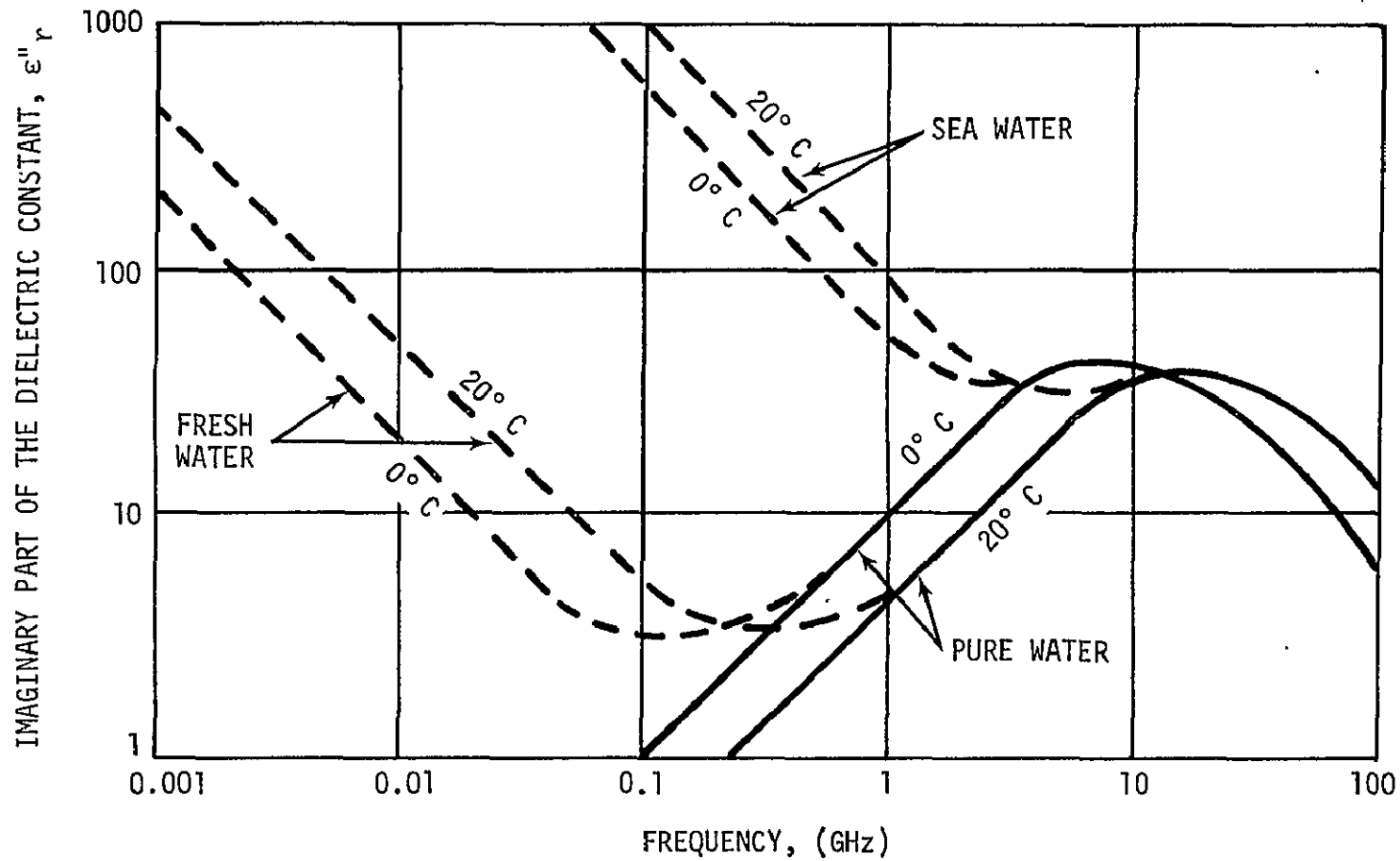


Figure 7. - Imaginary part of the complex dielectric constant of pure, fresh and sea water vs frequency for a water temperature of 0° C and 20° C (ref. 15).

4.3 DETERMINATION OF SURFACE PROFILE

The surface profile of the radar target determines the large scale and small scale roughness. For the SL-2 data site to be analyzed, the Gulf of Mexico was selected. The primary factor in determining the ocean's surface profile is the surface wind. From Phillips, (ref. 12) large-scale roughness is ascertained. J. Wu (ref. 13) has done detailed work relating wind velocity and ocean surface profile. From his work, the small scale roughness parameters were estimated. When determining the small scale roughness parameters, the following criteria were observed (ref. 2 and 9).

$$2\pi\sigma_{SS}/\lambda \ll 1$$

$$S_{SS}^2 = 2 \frac{\sigma_{SS}^2}{\lambda^2_{SS}} \quad (30)$$

assuming a Gaussian surface distribution.

The wind velocity history along the SL-2 FOV path prior to S-193 scatterometer measurements is not precisely known. According to NOAA weather data, wind velocities in the Gulf averaged approximately 11 knots during data acquisition for Pass 8, time slice 6. The following scatterometer backscatter calculation analysis gives some degree of sensitivity of σ° to ground truth accuracy.

Only large scale roughness at low incidence angles will be considered. For this case

$$\sigma^\circ = \frac{\sec^4 \alpha}{2S^2} |R(0)|^2 \exp\left(-\frac{\tan^2 \alpha}{2S^2}\right) \quad (31)$$

Let there be an error in the mean square slope because of erroneously estimating the wind velocity. Then the mean square slope will take on the incorrect value of $S^2 = S^2 \pm \Delta S^2$. A new σ° will be calculated ($\sigma^{\circ'}$) due to this incremental change in S^2 .

$$\sigma^{\circ'} = \frac{\sigma^\circ}{\left[1 \pm \frac{\Delta S^2}{S^2}\right] \exp\left[\left(\frac{-\tan^2 \alpha}{2S^2}\right)\left(1 \pm \frac{S^2}{\Delta S^2}\right)\right]} \quad (33)$$

Table VIII will indicate the error in σ° due to ground truth (wind speed) that is slightly in error.

A similar analysis could be done for small scale roughness and its effect on σ° . This type of analysis is applicable to land targets as well.

4.4 ATMOSPHERIC LOSSES

The rf link equation (9) which relates transmitted and reflected power from a target to received power does not include effects from atmospheric loss along the transmit and receive path. For the particular data sites selected to calculate σ° , and the corresponding value of P_R , there was little attenuation in the atmosphere. It was approximately 0.2 dB (ref. 2 and 6).

4.5 SL2/SL3 GROUND TRUTH

Figures 8 and 9 show the field-of-view (FOV) path for the S-193 scatterometer for both SL2 (ITNC Mode) and SL3 (ITC Mode) and accompanying wind speeds. These wind speeds

TABLE VIII. - SENSITIVITY OF σ° TO MEAN SQUARE
SURFACE SLOPE/WIND VELOCITY ERROR

Correct σ° (dB)	Calculated σ° from erroneous wind velocity (dB)	$\Delta\sigma^\circ$ (dB)	Correct S^2	ΔS^2	Correct wind velocity (knots)	Estimated wind velocity (knots)
16.02	16.02	0	0.032	0	10	10
16.02	15.09	-0.9	0.032	0.002	10	9
16.02	17.103	1.08	0.032	-0.002	10	11
16.02	13.52	-2.5	0.032	+0.006	10	13
16.02	19.66	3.64	0.032	-0.006	10	7

Note that the change in large scale roughness (ΔS^2) is a result of using an incorrect windspeed to calculate S^2 . This erroneous new S^2 gives a different σ° value.

were used to determine the sea surface profile and calculate a theoretical radar backscatter.

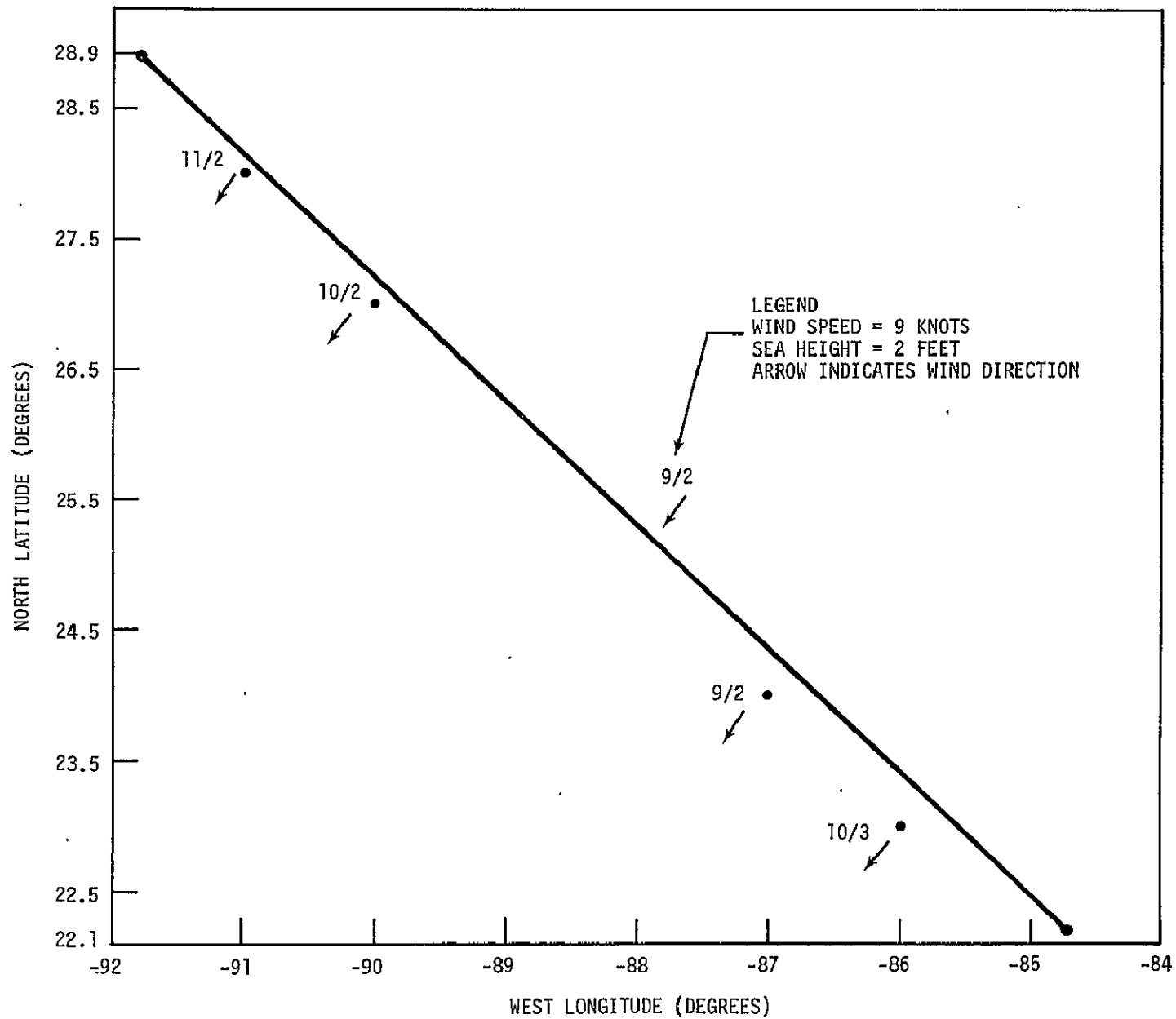


Figure 8. - FOV for S-193 EREP Pass '8 time slice 6, wind speeds, sea height and wind direction, operating mode = ITNC.

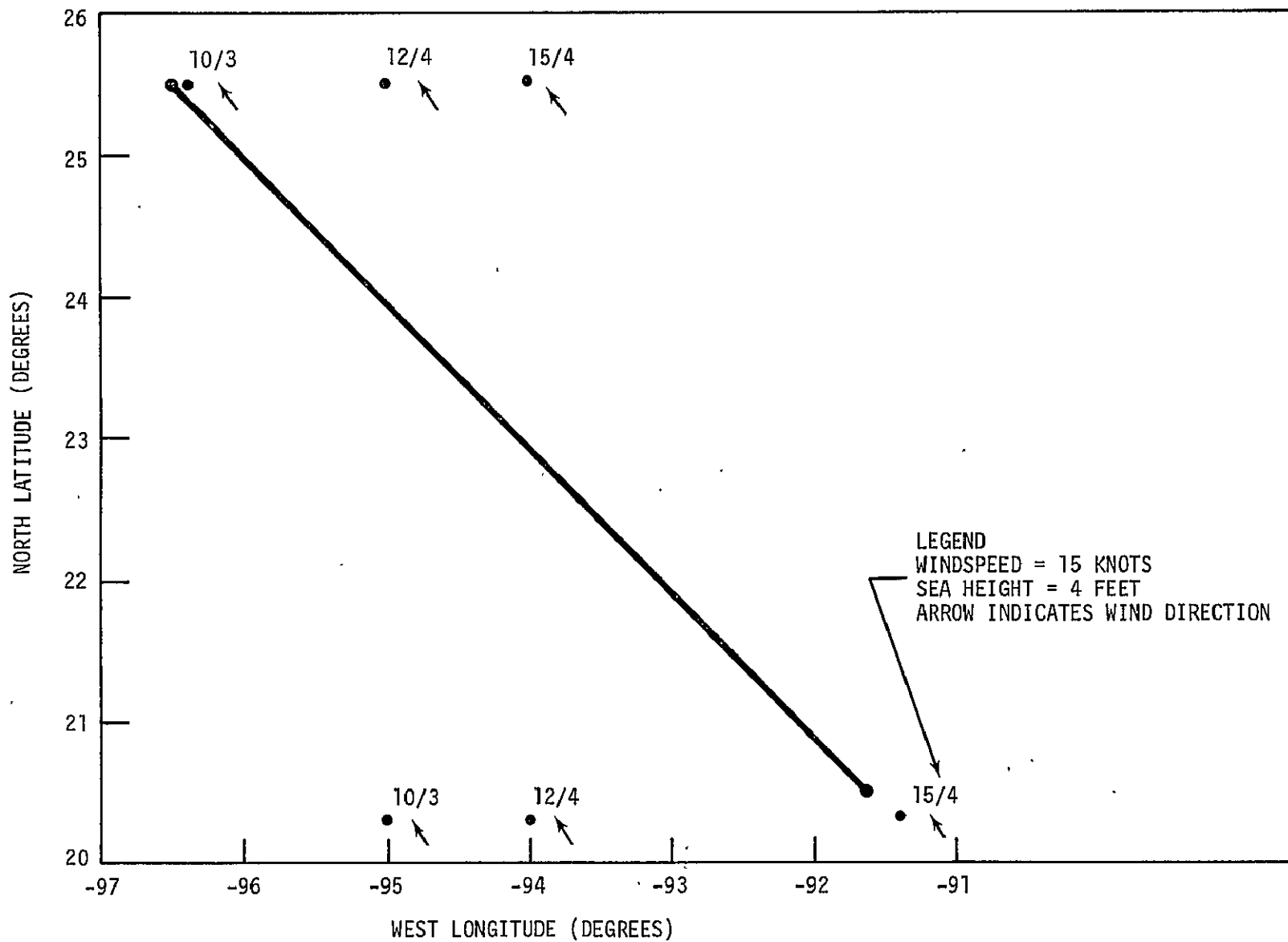


Figure 9. - FOV for S-193 EREP Pass 20 time slice 4, wind speed, sea height, wind direction, operating mode - ITC.

5.0 SKYLAB S-193 SCATTEROMETER

INPUT/OUTPUT CHARACTERISTICS

5.1 INTRODUCTION

For both SL2 and SL3, the following sections give the input/output (I/O) characteristics for the S-193 scatterometer. The input is in terms of the power received (P_R) at the S-193 parabolic antenna. The quantity P_R is determined from calculating σ° from the ground scene and utilizing the rf link equation (9). The output, in terms of millivolts (mv) into the integrator, is a measurement taken directly by the S-193 scatterometer. This quantity was selected to compare postflight data with preflight data that used voltage into the integrator as the output. Actually, the output of the S-193 system was in terms of counts from the A/D converter. In fact, the output of the whole system, as presented to the user, appears on paper products and tapes. From the I/O curves given in sections 5.2 and 5.3, the linearity and dynamic range of the S-193 scatterometer system itself will be evaluated. No attempt will be made here to assess the data handling beyond the output of the A/D converter. Also, in sections 5.2 and 5.3, system linearity will be studied by plotting the theoretical normalized radar cross-section versus S-193 calculated (measured) normalized radar cross-section.

The linearity and dynamic range of a system may be defined in several ways. For linearity, the output is linearly proportional to the input. Linearity can be expressed in terms of the maximum output of the instrument. This type of linearity is independent of the input and is based on a percentage of "maximum linear range" output.

Thus, 2 percent linearity means that the output will be within two parallel lines spaced ± 2 percent of the maximum output from the idealized output (ref. 14). In terms of the S-193 scatterometer linearity, the curves relating theoretical input (P_R) to measured output (V^*) and σ° theoretical VS σ° calculated will be used to assess linearity. Maximum output of the S-193 scatterometer system occurs at saturation, i.e., when the A/D converter output is 1023 counts for 5 volts into the A/D converter.

Dynamic range has a variety of definitions. The optimum output dynamic range is from a high value at saturation (A/D converter output is 1023 counts) to a low value where the noise measurement output of the A/D converter output is reached. Considering the A/D converter characteristics discussed in section 2.3, a "safety" factor of several counts should be added to the noise measurement counts out of the A/D converter. From the preflight curves, the 1 dB compression point below saturation for voltage into the integrator occurs at an input power (P_R) of -68 dBm. For saturation of the A/D converter the input power as read from the graph is -70 dBm. Therefore, the A/D converter is a determining factor in establishing the dynamic range of the S-193 scatterometer.

5.2 I/O CURVES FOR ITNC SL2 DATA

For the SL2 evaluation, ITNC scatterometer data taken over Gulf of Mexico was selected. The ground truth is given in section 4.3. For ground truth represented by an average wind speed of 11 knots and water temperature of 27°C, the theoretical I/O curve as shown in figures 10 and 11 is generated. Figure 11 shows the predicted σ° value versus the

S-193 measured σ° values. For each set of data modeled σ° values for VV, HH, HV, and VH polarization were predicted. Backscatter data for VV and HH polarization using equations (20), (21), (22), and (24) showed very little variation in composite σ° values when modeled. Therefore, only VV polarization backscatter was used in modeling. The cross polarized σ° model data was unusable in assessing S-193 scatterometer performance. Thus only σ_{VV}° values are predicted. Since there are five look angles or scan modes for the ITNC operating mode, when utilizing an "average" sea state, only five σ° values can be predicted theoretically. This is because there is only one set of large scale and small scale roughness parameters (e.g., S^2 , h^2 , ℓ^2) for an average sea state. The variable is the angle of incidence (α). For computing a theoretical σ° , four of the six parameters are used. In modeling the sea state, by varying the wind speed, which is analogous to a random sea surface profile, a large set of roughness parameters are generated.

In figure 10 the center of the crosses represents $\sigma^\circ_{\text{calculated}}$ versus $\sigma^\circ_{\text{measured}}$ values for an average sea state for one scan angle. The horizontal bars represent the variation in $\sigma^\circ_{\text{calculated}}$ for variation in wind speed of up to 11 ± 6 knots. The modeled values of σ° presented here are consistent with the typical σ° values presented in the literature. The vertical bars represent the variation in $\sigma^\circ_{\text{measured}}$ as given by the S-193 scatterometer data. To correlate these five predicted values to each of the five scan modes, the measured σ° values in a particular scan mode are averaged to give five average σ° values.

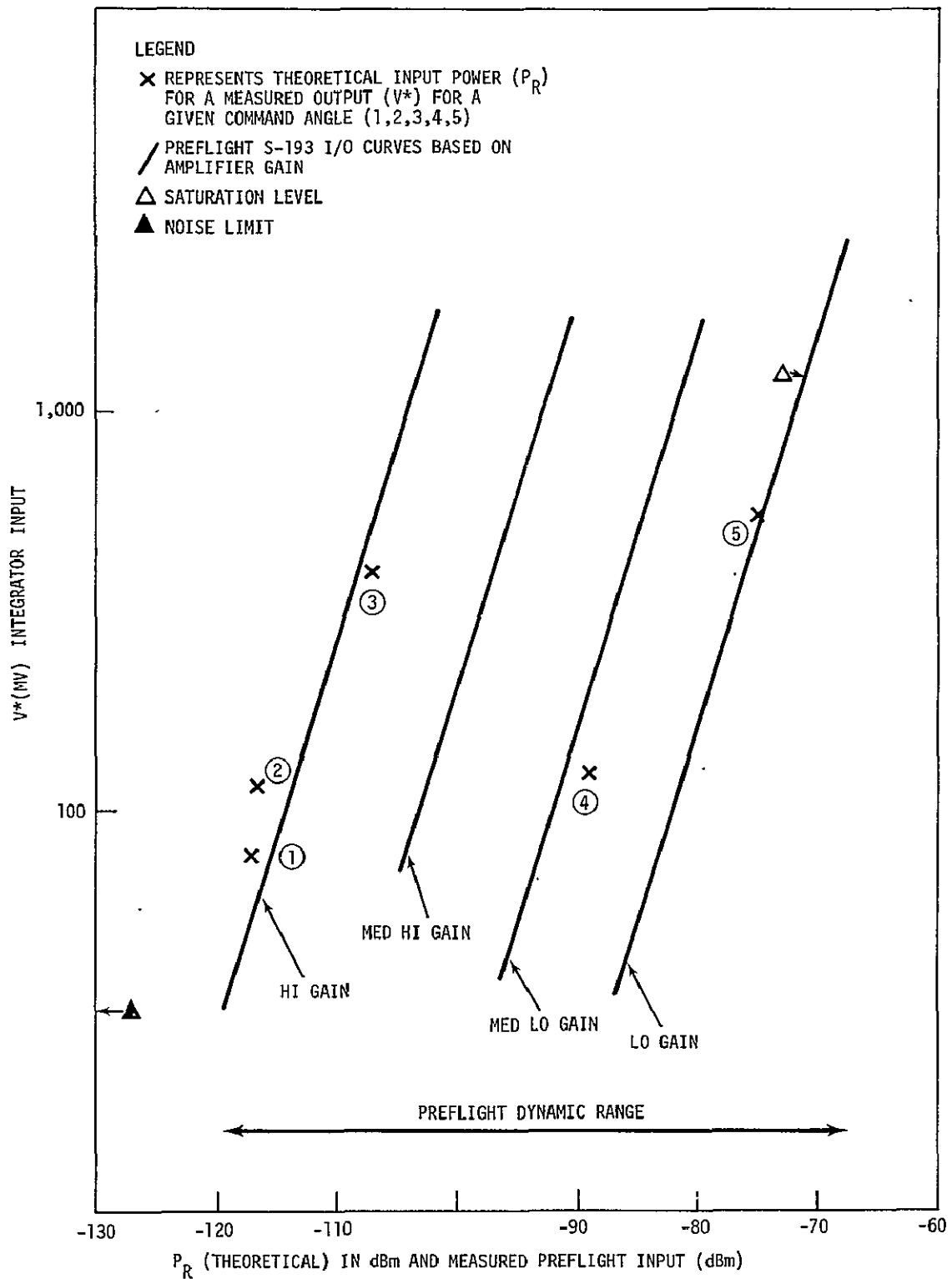


Figure 10. - S-193 I/O characteristics. Voltage into integrator (V^*) versus input power to antenna (P_R); EREP Pass 8 time slice 6 operating mode ITIVC.

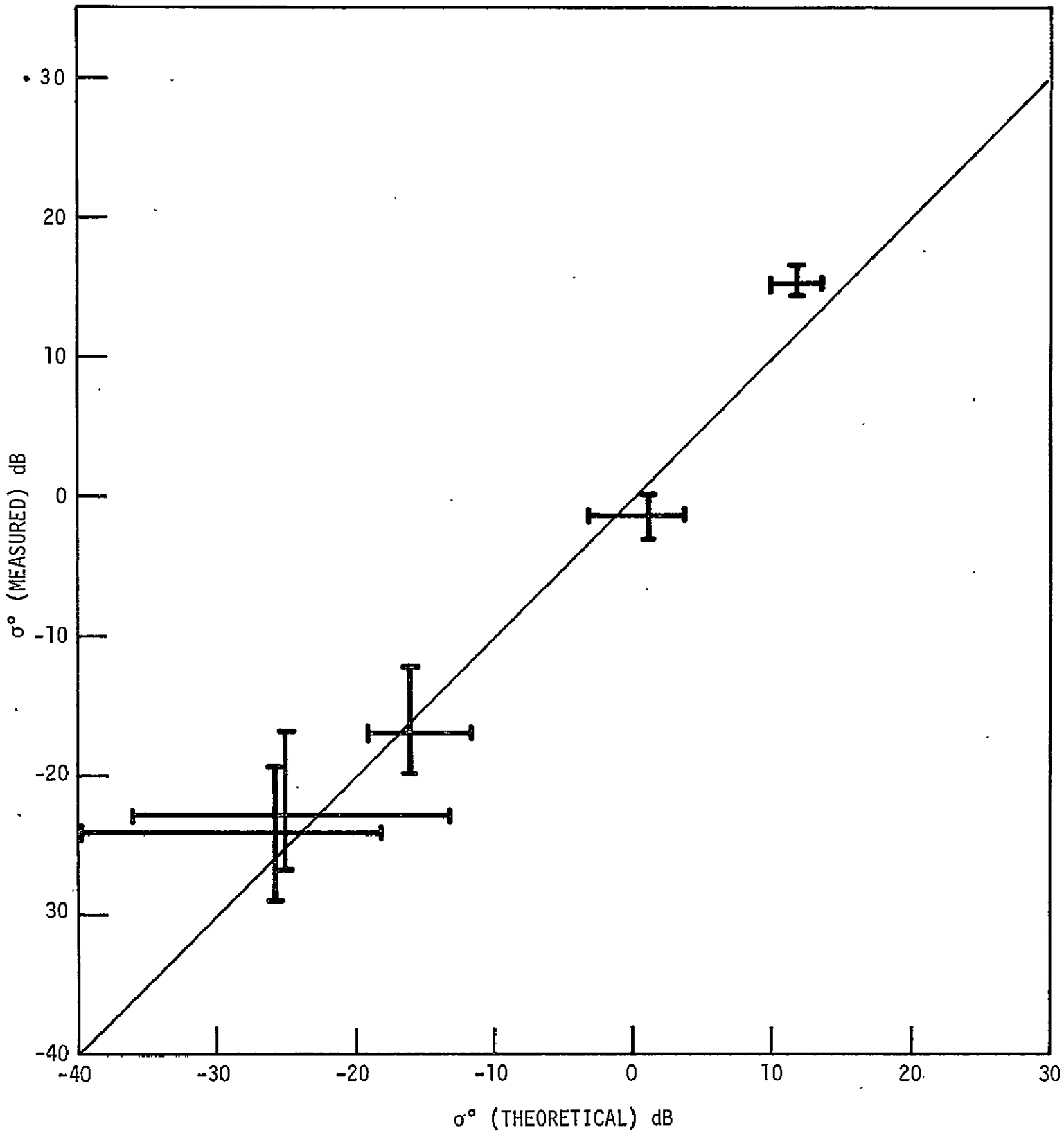


Figure 11. - S-193 theoretical backscatter vs measured backscatter
 EREP Pass 8, time slice 6, operating mode ITNC.

From figure 10, the dynamic range is approximately 49 dB. Saturation to high gain level noise outputs measurements are used as a criteria. If the "safety factor" for the A/D converter is considered for low signal-plus-noise to noise levels, the dynamic range is decreased about 1 to 2 dB. The preflight measured dynamic range was 50 dB for the S-193 scatterometer when using the MCF filter. This 50 dB range included mean noise and signal.

5.3 I/O CURVES OF SL3 ITC

Skylab 3 S-193 scatterometer performance was evaluated using ITC data taken over the Gulf of Mexico. The ground truth is given in section 4.3. For an average wind speed of 12.33 knots and water temperature of 30°C, the I/O curves shown in figures 12 and 13 are generated. These curves are for EREP pass 20 time slice 4, when the S-193 scatterometer was operating in the ITC mode. As for linearity of the ITC data, four of the five data points (MCF filter) were reasonably close to the idealized linearity curve. The one data point exception was for the scatterometer operation with the LCF filter. The gain curves were from preflight data for the MCF filter.

The dynamic range of the SL3 ITC data varies from $P_R = 69.5$ dBm at A/D converter saturation to -123 dBm. Thus the optimum dynamic range here is on the order of 53.5 dB. Figures 12 and 13 show $\sigma^{\circ}_{\text{measured}}$ versus $\sigma^{\circ}_{\text{calculated}}$ values and V^* versus P_R curves respectively. The output V^* is the voltage into the integrator.

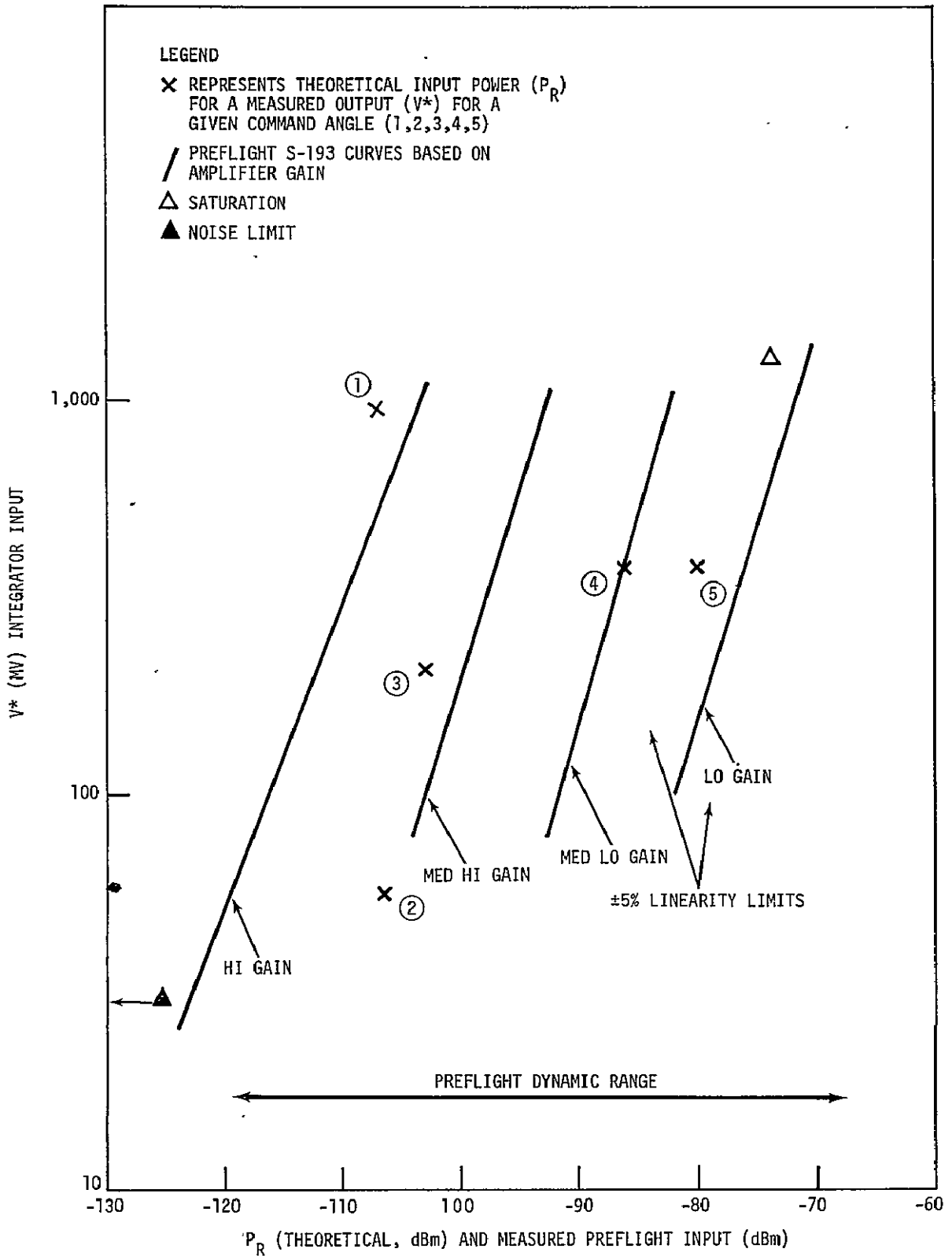


Figure 12. - S-193 I/O characteristics voltage into integrator (V^*), input power to antenna (P_R), EREP Pass 20, time slice 4, operating mode - ITC.

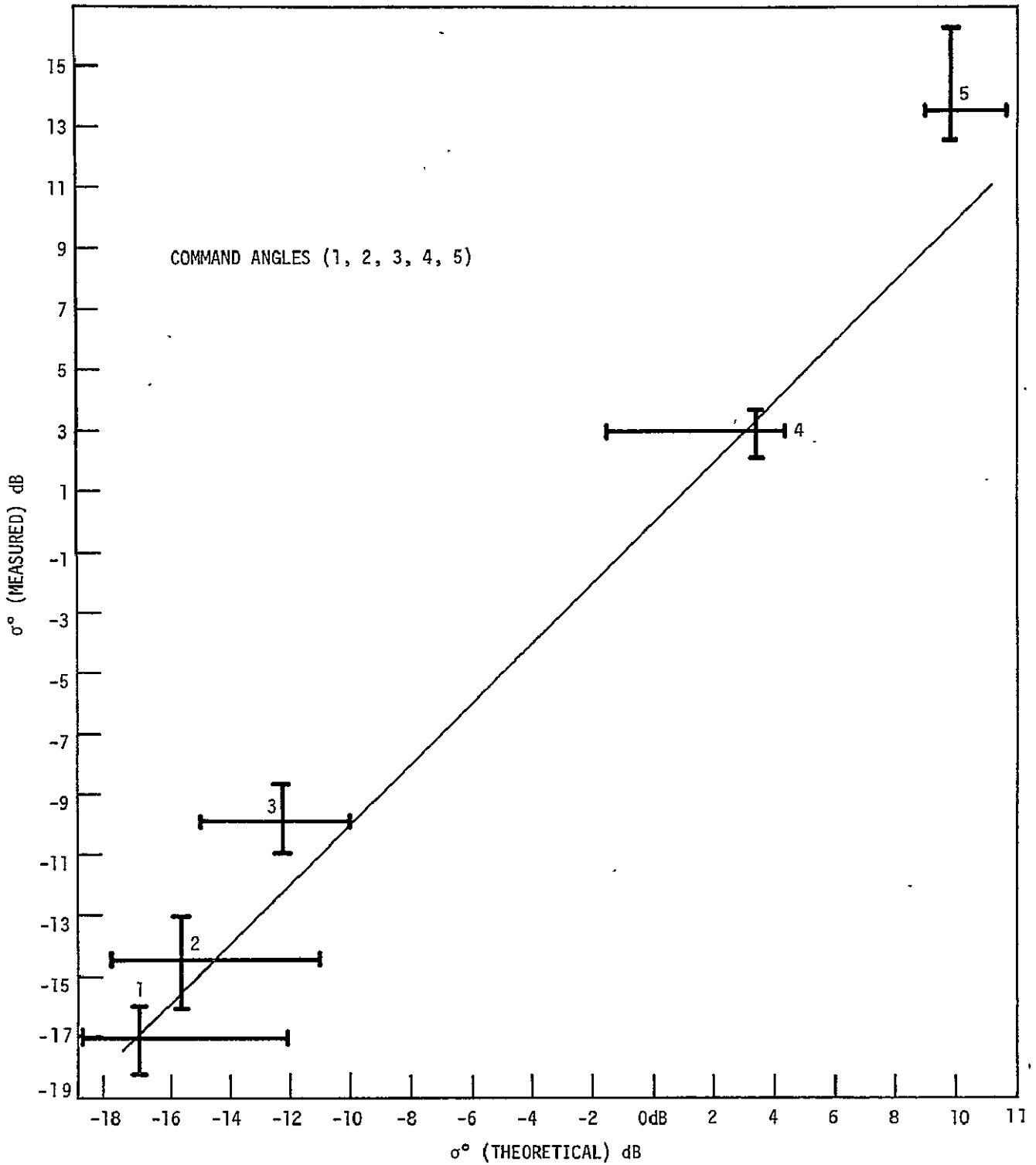


Figure 13. - S-193 theoretical backscatter vs measured backscatter, EREP Pass 20 time slice 4, operating mode ITC.

6.0 CONCLUSIONS

From the results of section 5, the performance of the S-193 scatterometer in both SL2 and SL3 did not vary appreciably from that recorded in preflight tests. Nor was there much indicated variation between SL2 and SL3 operation of the S-193 when evaluating the ITNC and ITC data presented in section five. Upon examining figures 10 through 13, it seems that the operation of the scatterometer is linear. This linearity depends not only upon the measured value of σ° but also upon the predicted value of received power (P_R). A numerical evaluation of linearity is limited due to constraints in radar cross section modeling and ground truth.

The dynamic range of the instrument is on the order of 50 dB. However, it should be noted that the lower cut-off value of the dynamic range will vary slightly from pass to pass and time slice to time slice. This is due to variation in the noise for high gain amplification measurement from time slice to time slice. In high gain operation, within any one-time slice, the noise level measured varies only a few counts. The measured noise is a function of emission from the radar target and other sources as well as system noise.

7.0 REFERENCES

1. Krishen, K. and Pounds, D. J.: Evaluation Implementation Plan. LEC-640, TR-179, Lockheed Electronics Company, Inc., JSC-SPE-00413, May 1973.
2. Kaufman, D. E.: RF Link Equation For The Skylab S-193 Radiometer/Scatterometer, LEC-4119, Lockheed Electronics Company, Inc., Contract NAS 9-12200, August 1974.
3. Anon.: Calibration Data Report, S-193 Microwave Radiometer/Scatterometer Altimeter, General Electric Corporation, Contract NAS 9-11195, October 1974.
4. Krishen, K. and Pounds, D. J.: S-193 Radiometer and Scatterometer Sensor Mathematical Models. LEC-1741, Lockheed Electronics Company, Inc., Contract NAS 9-12200, February 1974.
5. Anon.: Earth Resources Production Processing Requirements for EREP Electronic Sensors. National Aeronautics and Space Administration/Johnson Space Center, Document Number TR524, May 1973.
6. Skolnik, M. I.: Radar Handbook. McGraw-Hill, New York, 1970.
7. Sobti, A. and Cook, A. C.: Towards More Precise Production of S-193 Data. Technical Memorandum 236-6, University of Kansas Space Technology Laboratories, Lawrence, Kansas, August 1973.
8. Barrick, D. E.: Radar Cross Section Handbook. Plenum Press, New York, 1970.
9. Beckmann, P. and Spizzichino, A.: The Scattering of Electromagnetic Waves From Rough Surfaces. Pergamon Press, New York, 1963.
10. Paris, J. F.: Microwave Radiometry and Its Application to Marine Meteorology and Oceanography. Texas A&M Research Foundation, Project 286-13, January 1969.
11. Pierson, W. J. and Neumann, G.: Principals of Physical Oceanography. Prentice-Hall, Inc., New Jersey, 1966.

12. Phillips, O. M.: The Dynamics of The Upper Ocean. Cambridge Monographs On Mechanics and Applied Mathematics, Cambridge Press, 1966.
13. Wu, J.: Sea-Surface Slope And Equilibrium Wind-Wave Spectra. The Physics Of Fluids, Vol. 15, No. 5, May 1972.
14. Cook, N. H. and Rabinowicz, E.: Physical Measurement and Analysis, Addison-Wesley Publishing Co., Inc., California, 1963.

APPENDIX

The following two sets of tables show the maximum/
minimum σ° value for SL2/SL3 scatterometer data.

TABLE A-I. - SL-2 DATA

EREP Pass No./ Time Slice	Mode	Polz	Max σ° dB	Min σ° dB	$\Delta\sigma^\circ$ dB
1/2	ITNC	VV	-13.71	-28.16	14.45
2/2	ITC	VV	-2.43	-13.76	11.33
2/3	ITC	HH	8.55	-9.6	18.15
3/1	CTC	VV	-4.72	-15.77	11.05
3/2	ITC	VV	5.57	-12.92	18.49
4/1	ITC	VV	18.73	-13.14	31.87
5/1	CTC	VV	16.04	-7.48	23.52
5/2	ITC	VV	7.08	-16.67	23.75
5/3	CTC	VV	-7.38	-11.46	4.08
5/4	ITNC	Sequence	16.81	-42.97	59.78
5A/1	CTNC	Sequence	14.13	-33.95	48.08
6/2	CTC	VV	-5.31	-11.32	6.01
6/3	ITC	VV	19.6	-11.82	31.42
6/4	ITC	HH	8.5	-22.15	30.65
7/1	ITC	VV	5.70	-15.59	21.29
7/2	ITC	HH	5.69	-23.13	28.82
7/3	CTC	Sequence	-4.66	-33.22	24.66
8/1	CTC	VV	-7.89	-12.67	4.78
8/2	ITC	VV	1.89	-13.66	15.55
8/3	ITC	VH			
8/4	ITC	HH	5.11	-14.78	19.97
8/5	ITC	HV	-3.5	-18.78/ -42.1	15.28/ 38.6
8/6	ITNC	Sequence	16.47	-45.67	62.14
8/7	ITNC	Sequence	14.54	-46.21	60.75
8/8	CTC	HH/VV	-4.83	-11.77	6.94
8/9	CTC	HH	-7.23	-7.98	2.75
9/1	ITNC	Sequence	14.91	-35.8	50.71

TABLE A-I. - SL-2 DATA - Concluded.

EREP Pass No./ Time Slice	Mode	Polz	Max σ° dB	Min σ° dB	$\Delta\sigma^\circ$ dB
10/1	ITNC	Sequence	-20.1	-63.57	43.47
10/2	ITNC	HH	4.07	-73.92/ -60.3, -30.66	77.99/ 34.73
10/3	ITNC	HH	11.45	-36.29	47.74
10/4	ITNC	HH	-39.27	-43.26	3.99
10/9	CTC	VV	20.66	-13.21	33.87
10/10	CTC	HH	20.45	-6.46	26.91
10/12	CTC	HH	-6.73	-9.21	2.48
10/13	CTC	VV	-6.1	-9.76	3.66
10/14	CTC	VV	-5.83	-47.14	41.31
11/3	ITC	VH	-3.85	-42.60 Gulf	38.75
11/4	CTC	VV/HH			<2
LC1/1	Rad only				
LC1/2	No S062-C				
LC1/3	1 data point nonzero at -40.87				
LC1/4	CTC	VV	-33.67	-48.06	14.39
LC1/5	ITC	VV	-38.14	-51.46	13.32
LC1/6	ITNC	Sequence	-37.83	-52.47	14.64
LC1/8	CTNC	Sequence	-33.14	-51.72	18.58

TABLE A-II. - SL-3 DATA

EREP Pass No./ Time Slice	Mode	Polz	Max σ° (dB)	Min σ° (dB)	$\Delta\sigma^\circ$ (dB)
12/1	CTC R/S	HH	14.11	6.74	7.37
12/2	CTC R/S	VV	16.1	-9.41	25.51
12/3	CTC R/S	VV	-7.22	-26.53	19.31
12/4	CTC R/S	HH	-6.59	-12.57	5.97
12/5	CTC R/S	HH	16.43	-6.38	22.81
12/6	CTC R/S	VV	14.39	-8.79	23.18
12/7	CTC R/S	VV	13.70	7.14	6.56
12/8					No data
12/9	CTC Scat	HH	-5.16	-9.05	3.89
13/1	CTNC R/S	Sequence	13.26	-35.66	48.92
13/2	ITNC R/S	Sequence	13.39	-33.11	46.5
13/3	CTC R/S	VV	-1.90	-9.52	7.62
13/4	CTC R/S	HH	-2.41	-9.40	6.99
13/5	CTC R/S	HH	17.34	-11.96	29.30
13/6	CTC R/S	VV	20.91	-6.48	27.39
13/7	CTC Scat	HH	-5.55	-6.07	0.52
13/8	CTC R/S	VV	-6.51	-10.86	4.34
14/1	ITNC R/S	Sequence	14.47	-41.90	56.37
14/2	ITNC R/S	Sequence	-8.12	-27.21	19.09
15/1	ITNC R/S	HH	14.71	-13.88	28.59
15/2	ITNC R/S	VV	8.86	-44.17	53.03
15/3	CTC R/S	VV	-6.99	-12.35	5.36
15/4	CTC Scat	VV	16.79	-7.28	24.07
15/5	CTC R/S	VV	14.56	-5.41	19.97
15/6	CTC R/S	HH	6.17	-7.12	13.24
15/7	CTC Scat	HH	-4.70	-12.94	8.29
15/8	CTC R/S	VV	-7.58	-11.15	3.57
15/9	CTC R/S	HH	-7.51	-10.09	2.58
15/10	CTC R/S	HH	-4.57	-48.14	43.57

TABLE A-II. - SL-3 DATA - Continued

EREP Pass No./ Time Slice	Mode	Polz	Max σ° (dB)	Min σ° (dB)	$\Delta\sigma^\circ$ (dB)
16/1	CTNC 4R2/5	Sequence	14.38	-43.89	58.27
16/2	ITNC R/S	Sequence	17.79	-44.54	62.33
16/3	CTC R/S	VV	-2.17	-19.54	17.37
16/4	CTC R/S	VV	-8.81	-11.72	2.91
16/5	ITNC R/S	VV	14.13	-24.82	38.95
16/6	CTNC L R/S	VV	14.59	-32.70	47.29
16/7	CTNC L R/S	VV	2.10	-26.92	29.02
16/8	CTC Scat	VV	24.99	-11.86	36.85
16/9	CTC R/S	VV	-4.32	-25.64	20.82
17/1	CTC R/S	VV	15.36	-9.45	24.81
17/2	CTC R/S	HH	19.60	-7.57	27.17
17/3	ITNC R/S	Sequence	14.73	-34.14	48.37
17/4	ITNC R/S	Sequence	-6.16	-14.62	8.46
18/1	ITC R/S	HH	5.98	-50.53	56.51
18/2					No data
18/3	CTC Scat	VV	-3.96	-45.24	41.28
18/4					No data
18/5	CTC Scat	HH	-4.49	-10.28	5.79
19/1	CTC R/S	HH	-3.60	-23.06	19.46
20/1	ITC R/S	HH	13.80	-16.09	29.89
20/2	CTC R/S	VV	0.71	-10.78	11.49
20/3	ITC R/S	VV	7.38	-41.96	49.34
20/4	ITC R/S	VV	15.89	-50.47	66.36
20/5	CTC Scat	HH	-5.27	-10.84	5.57
LC Data					
21/1	CTC R/S	HH	20.90	-13.19	34.09
21/2	CTC R/S	HH	19.60	-34.36	53.96
21/3	CTC R/S	VV	17.69	-4.80	22.49

TABLE A-II. - SL-3 DATA - Concluded

EREP Pass No./ Time Slice	Mode	Polz	Max σ° (dB)	Min σ° (dB)	$\Delta\sigma^\circ$ (dB)
22/1	CTC R/S	HH	19.80	-10.55	30.35
22/2	CTC R/S	HH	17.74	-6.00	23.74
22/3	CTC R/S	HH	18.58	-5.27	23.85
23/1	CTNC L R/S	Sequence	14.16	-53.48	67.64
24/1	CTC R/S	VV	-9.27	-24.37	15.16
26/1	CTNC R/S	Sequence	18.20	-49.37	67.57
27/1	CTC R/S	VV	6.43	-18.03	24.46
27/2	CTC R/S	HH	18.21	-17.32	35.53
28/1	CTC R/S	VV	-5.36	-34.68	29.32
28/2	ITC R/S	VV	7.73	-14.24	21.97
28/3	ITC R/S	HH	13.12	-10.70	23.82
29/1	ITNC R/S	Sequence	18.76	-63.17	81.93
30/1	ITC R/S	VV	13.62	-15.52	29.14
31/1	CTC R/S	VV	20.85	-7.05	27.90
31/2	CTC R/S	HH	21.37	-14.41	35.78
31/3	CTC R/S	VV	21.31	-10.42	31.55
31/4	CTC R/S	VV	-5.71	-14.16	8.45
31/5	CTC R/S	VV	8.58	-8.63	17.21
31/6					No data
32/1	ITC R/S	VV	1.62	-10.79	12.41
LC3 Data					
34/1 to 35/7					No data
38/8	CTC Scat	VV	14.45	-6.55	21.00
39/1	ITC R/S	VV	18.13	-12.19	30.32
39/2	ITC R/S	HH	12.84	-10.23	23.07
40/1	CTC R/S	VV	-5.66	-15.36	9.70
40/2	ITC R/S	VV	12.86	-53.14	66.00
43/1	CTC R/S	VV	-32.74	-44.16	11.41
43/2	ITC R/S	VV	-14.12	-35.48	21.36
43/3	CTC Scat	VV	-30.58	-46.16	15.58
43/4					No data
43/5	ITC R/S	VV	-16.53	-35.74	19.21
43/6					No data